ENHANCED ADDRESSABILITY AND LOCALIZATION IN DIGITAL MICROFLUIDIC MULTIPLEXER SYSTEMS

by

Milad Abolhasani

B.Sc., Sharif University of Technology, Iran, 2008

A THESIS SUBMITTED IN PARTIAL FULFILLMENT OF
THE REQUIREMENTS FOR THE DEGREE OF

MASTER OF APPLIED SCIENCE

in

The College of Graduate Studies

(Mechanical Engineering)

THE UNIVERSITY OF BRITISH COLUMBIA
(Okanagan)

April 2010

Abstract

This research presents a novel digital microfluidic multiplexer structure based on a cross-referencing architecture. The new multiplexing technique uses bi-polar voltage activation and threshold effects to overcome addressability limitations and eliminate inter-microdroplet interference.

Fan et al. [1] introduced cross-referencing for enhancing addressability. The technique uses two sets of rectangular electrodes: top rows and bottom columns. Such a system achieves $m{\times}n$ addressability with only $m{+}n$ electrodes. This is a significant achievement as voltage addressing and microdroplet actuation are performed by the same linear electrode structures.

There remains one major drawback to the conventional cross-referencing method. Desired motion of a microdroplet on an electrode grid can result in undesired motion of other microdroplets placed on the same electrode row. Fan et al. [2] and Xu and Chakrabarty [3] have proposed intriguing solutions to this problem with cascaded differential voltage activation and graph theory, respectively. However, these methods become increasingly complex for systems with multiple microdroplets, as the solutions for addressability must have a limited number of microdroplets.

The proposed method introduces a new multiplexing format for cross-referencing of DMF systems through the simultaneous use of threshold-based voltage actuation (which sets a minimum voltage to initiate microdroplet motion) and bi-polar voltage activation on the overlying and underlying electrodes. The threshold voltage effect for requirement one has been characterized numerically and experimentally, and the results are presented here. With regard to requirement two, it is necessary to employ a voltage addressing scheme that can preferentially isolate overlapped regions of the 2-D grid. This goal can be achieved using a bi-polar electrode activation technique, as the bi-polar DMF multiplexers will have a $\pm 2V_{app}$ voltage difference in the overlapped location and only a maximum of $\pm 1\ V_{app}$ voltage difference in all other locations.

This relationship has been quantified using an electrostatic 3-D COMSOL model of the proposed DMF multiplexer.

A fabrication recipe for the proposed DMF multiplexer system is reported in this research, and the multiplexing protocol has been studied experimentally to verify the numerical analyses. The proposed technique with this threshold-based bi-polar activation can improve $m \times n$ addressability with multiple microdroplets in a cross-referenced DMF grid.

Table of Contents

List of Tables

List of Figures

Acknowledgments

First the foremost, I would like to thank my MASc supervisors, Dr. Homayoun Najjaran, Dr. Mina Hoorfar and Dr. Jonathan F. Holzman, for their understanding, encouragement, support, enthusiasm, and guidance. Your helpful suggestions and patient conductions have gone through all my works in the past two years. I attribute the level of my Masters degree to their encouragements and efforts, and without them this thesis would not have been completed.

Also, I would like to express my thanks to the following advisory committee members: Dr. Rudolf Seethaler and Dr. Peter Hallschmid. Thanks also go to Dr. Axel Guenther, from University of Toronto, for his willingness to serve as my external examiner. I really appreciate their valuable time and constructive comments on my thesis.

I would like to thank my dear colleagues Ali Ahmadi and Morteza Farrokhsiar for all of their assistances, encouragements and supports during my two-year study at the University of British Columbia Okanagan.

Finally, special thanks are owed to my parents and my sister for their patience and moral supports over all these years of education. Without their constant support and encouragement, all my achievements would not be possible.

Dedications

THIS THESIS IS DEDICATED TO MY FAMILY…
FOR ALL OF THEIR LOVE AND SUPPORT

Chapter 1

1.1   Introduction

In the last few decades microfluidic topics have drawn a lot of researchers' attention in chemistry [4], biology [5, 6] and health science [7, 8] fields. Lab-on-a-chip (LOC) devices, for example, have been particularly successful in operating with a variety of liquids and in performing numerous analytical tasks.

From a structure and design point of view, there are two different microfluidic architectures: continuous and digital. The digital microfluidic (DMF) architectures use localized actuation forces in order to address and move discrete microdroplets on the chip. Compared to continuous microfluidics with micro-channels, micro-valves and micro-pumps, DMF devices have demonstrated reduced limitations in terms of fatigue, bubble creation, leakage and clogging.

The manipulation of small liquid volumes has many advantages in biological and chemical applications. Research efforts have demonstrated this manipulation through numerous actuation mechanisms, including piezoelectric [9], electrostatic [9], thermopneumatic [10], electrophoresis [10], dielectrophoresis [10], shape memory alloy [11], bimetallic [11], electroosmotic [11], and electromagnetic [11]. Most of these efforts are based on liquid flow in microchannels with many mechanical parts. Also, by transferring from macro-scale to micro-scale, surface forces are dominant to volume forces. Therefore, large devices are particularly ineffective at making efficient use of surface forces on micron scales. In fact, actuation methods that do not require moving parts are highly desirable.

There are numerous methods for actuating microdroplets in DMF devices. The vast majority of these techniques have employed thermocapillary or electrocapillary effects. Compared to thermal control of surface tension, however, electrical control is especially energy efficient in providing microfluidic actuation [9]. For example, Pollack et al. [12] have demonstrated electrostatic actuation based on voltage-dependent surface tensions for actuation of discrete microdroplets. Similarly, Ding et al. [13] reported a new architectural design and methodology for scheduling biochemical reactions in an electrode array using electrowetting. These results were improved further by Cho et al. [14] in the successful demonstration of electrowetting on a

dielectric (EWOD) by performing splitting, merging, creating and moving microdroplets in a system covered with dielectric layers.

The interest in DMF stems from its many advantages summarized in the following [4] :

- **Operation without permanently-etched channels:**

There are no physical channels in DMF devices for microdroplet motion. Instead virtual channels can be imagined in the DMF control structure.

- **Operation without moving parts:**

There are no moving parts in DMF devices, so there is a reduced risk of system errors related to valve clogging or wear.

- **Reduced reagent volume:**

The micron scale of the samples and reagents has the potential to improve the device efficiency and operational costs compared to macro scale devices.

- **Simultaneous control:**

Because the actuation mechanism in DMF devices is localized, multiple microdroplets can be simultaneously manipulated.

- **Operation with numerous types of liquid:**

Analytical fluid processes can be carried out with a variety of fluids in DMF devices.

- **Visualization:**

DMF devices allow for real-time monitoring of microdroplet motion without CCD cameras.

- **High energy efficiency:**

Power consumption of DMF devices is extremely small (i.e. 1-1000 nW).

- **Improved flexibility:**

The generalized structure of DMF chips allows these systems to be easily reconfigured and controlled by adapting the software of the control system rather than restructuring the entire system.

With the above advantages, DMF is a promising area with many applications in biochemistry and biosensors (LOC, immunoassays), DNA analysis [15], DNA repair microprocessor, cell-on-a-chip [16], cell sorting and polymerase chain reaction (PCR) [17].

1.2   DMF Systems

From the structure point of view, DMF systems using electrowetting can be classified into three different groups: Open, closed and cross-referencing DMF systems. The following subsections provide a brief introduction to each of these structures and discuss their challenges.

1.2.1 Open DMF System

Open systems (or catena wire systems) consist of underlying electrodes and an overlying catena wire [18-20]. Typically the bottom electrodes are covered with a hydrophobic layer (e.g., Teflon or polydimethylsiloxane (PDMS)), and the catena wire is inserted into the microdroplet from above. The contact angle for this static case can be linked to the surface tensions through Young's equation [21]:

$$\gamma_{LG} \cos(\theta) = \gamma_{SG} - \gamma_{SL},\tag{1}$$

where, θ is the contact angle, γ_{LG} is the liquid-gas surface tension, γ_{SG} is the solid-gas surface tension, and γ_{SL} is the solid-liquid surface tension. These variables are shown in Figure 1.1.
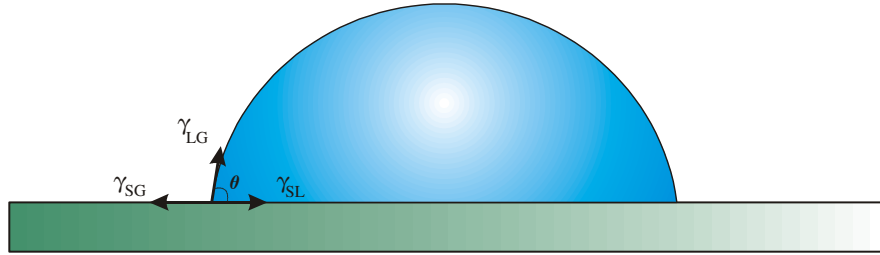
Figure 1.1 Surface tensions at the three-phase contact line of a microdroplet.

By applying a DC or AC voltage to the bottom electrodes and grounding the catena wire, free charges accumulate at the interface of the microdroplet, and the hydrophobic layer is polarized. The resulting induced electric fields will be coupled to the interfacial charges to apply an interfacial force and deform the interface. The dependency of contact angle change to applied voltage can be explained by the Lipmann-Young equation [12]:

$$\cos(\theta) = \cos(\theta_0) + \frac{C}{2\gamma_{LG}} V^2,\tag{2}$$

where θ_0 is the initial contact angle before applying the voltage, C is the capacitance per unit area of the electrical double layer and hydrophobic layer and V is the voltage applied to the bottom electrode (Figure 1.2).
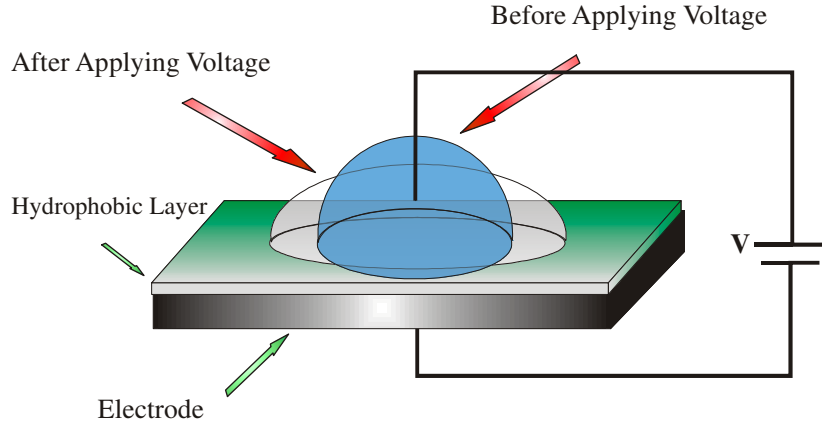
Figure 1.2 Schematic of an open DMF system without dielectric layer (electrowetting).

Direct electrowetting in an open DMF system has numerous limitations, including high electric currents and contact angle saturation. To overcome or reduce some of these limitations, a dielectric layer has been added to the previous open DMF systems and resulting technique is called EWOD [22] (see Figure 1.3). In this type of electrowetting, the added dielectric layer results in lower electric current and power consumption, but higher potential voltages. In this case, the capacitance in the Lippmann-Young equation is dominated by the capacitance of the dielectric layer (as it is much higher than the capacitance of the double layer) [21].
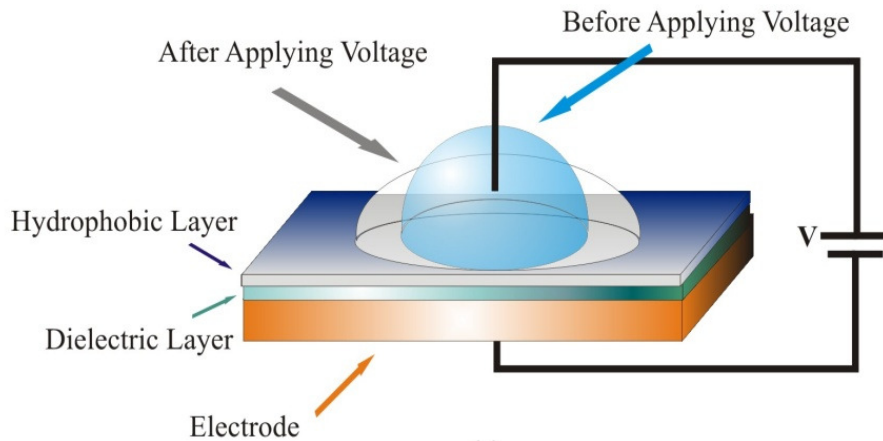
Figure 1.3 Schematic of an open DMF system with a dielectric layer (EWOD).

1.2.2 Closed System

In order to overcome practical limitations of the open DMF systems (e.g., evaporation), the second generation of DMF systems, called closed systems, was developed [21]. In closed electrowetting or EWOD systems, microdroplets are encapsulated between two plates. Spacers are used to define the gap height between the two plates. The schematic of this system is shown in Figure 1.4. The filler fluid surrounding the microdroplet can be air or silicone oil. Compared to air, silicone oil provides easier motion, smaller microdroplet edge hysteresis, lower actuation voltages, and negligible evaporation rates [12].
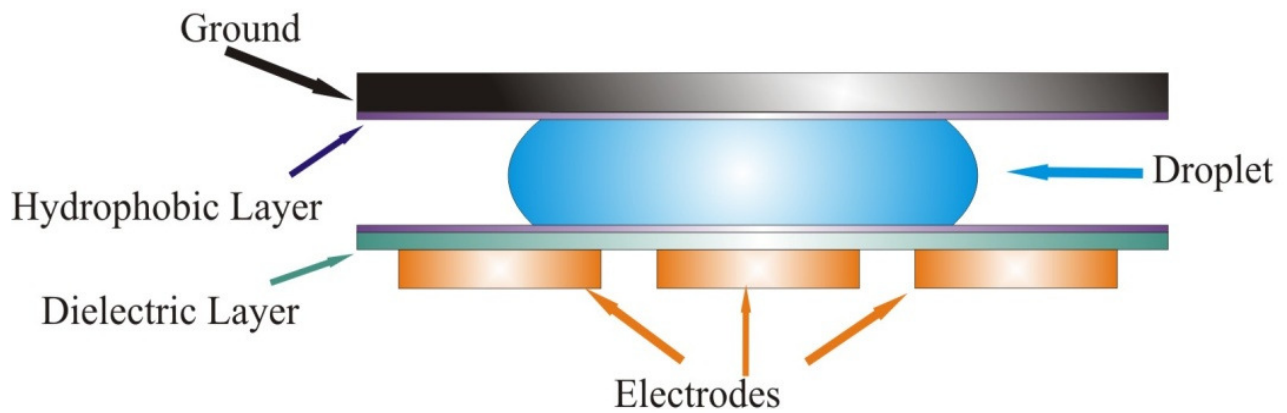
Figure 1.4 Schematic of a closed DMF system.

1.2.3 Cross-Referencing System

Both of the DMF systems described in the previous two subsections are limited in complexity as they are based on simple architectures. The tasks (e.g. merging, splitting and creating) that these simple systems can perform are therefore somewhat restricted, as such systems are fundamentally limited by electrode addressability issues. The need to contact electrically individual inner electrodes in the 2-D plane without shorting, overlapping, or crossing the address lines can become extremely difficult for systems with high levels of complexity [1, 2].

Fan et al. [1] proposed a new method for solving the addressability issue of the electrodes by using two sets of rectangular electrodes. The method is called cross-referencing. In these systems, separated electrodes are overlapped and oriented orthogonally with microdroplet motion induced between the overlying top electrode plates and underlying bottom electrode plates. This is shown in Figure 1.5. Such a system can achieve $m{\times}n$ addressability with only $m{+}n$ electrodes. This is a significant achievement as the voltage addressing and microdroplet actuation are performed by the same linear electrode structures. As a result, the operational complexity can be greatly reduced from that of the 2-D individually addressed electrode arrays.
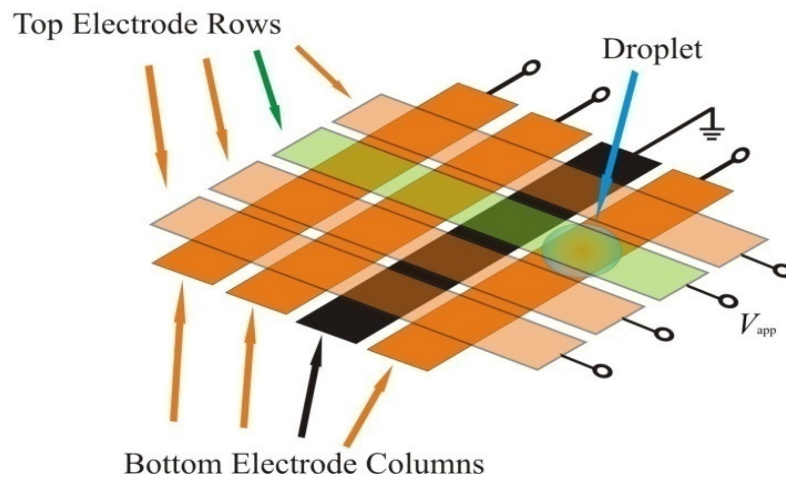
Figure 1.5 Schematic view of a cross-referencing system.

1.3   Proposed Multiplexer

While cross-referencing can allow for simplified addressing, there are fundamental limitations in the ability of such systems to operate with multiple microdroplets [2]. One of these limitations is shown in Figure 1.6. The desire to actuate only one microdroplet becomes difficult in a multiple microdroplet system, as all microdroplets experiencing a net applied voltage will start to move. For example, applying a voltage to a particular top row with two microdroplets positioned below it will simultaneously actuate both microdroplets (even if this simultaneous motion is not desired). Clearly, the addressability of these cross-referencing systems must be improved, and research groups have had limited success at this.
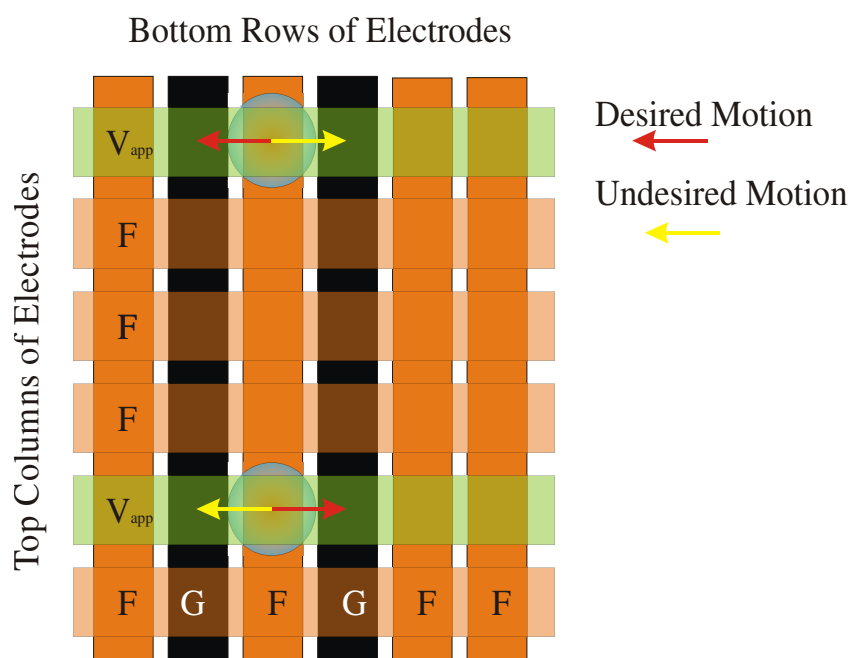
Figure 1.6 One of the cross-referencing method limitations.

This research focuses on a novel DMF multiplexer protocol that overcomes the aforementioned limitation of cross-referencing systems in certain configurations. The proposed method will introduce a new multiplexing format for cross-referencing DMF systems. The fundamental operation of these DMF multiplexers will make use of a cross-referencing architecture and bi-polar voltage activation. This is shown in Figure 1.7. This new form of bi-

polar electrode activation can be used to accentuate threshold-voltage effects of the fluid motion. The DMF multiplexers will be designed such that motion is induced only in regions where the overlying top electrodes (with +*V*) overlap the underlying bottom electrodes (with −*V*). A threshold condition is used to ensure that only the 2*V* voltage difference in this location can cause the microdroplet motion. Regions experiencing only ±*V* voltage differences will not overcome the threshold voltage condition and will not induce motion. This technique will be the first of its kind and is expected to allow for *m*×*n* addressability with multiple microdroplets and only *m*+*n* electrodes.

(a)

Top Columns of Electrodes

Dielectric Layer

+V_{app}

Hydrophobic Layer

Droplet

-V_{app}

Bottom Rows of Electrodes

(b)
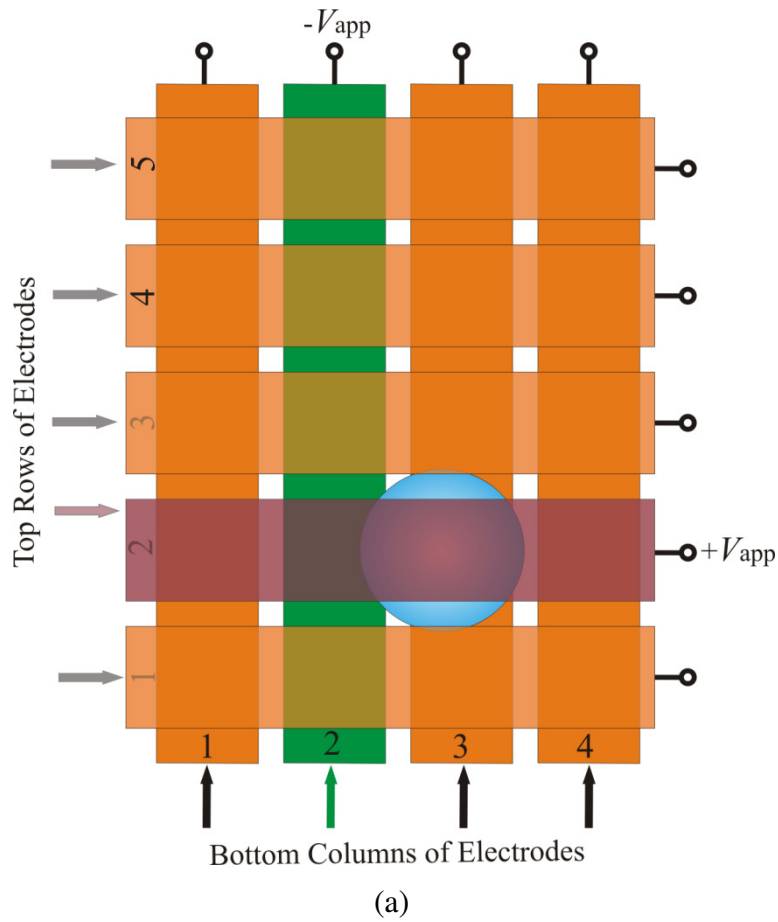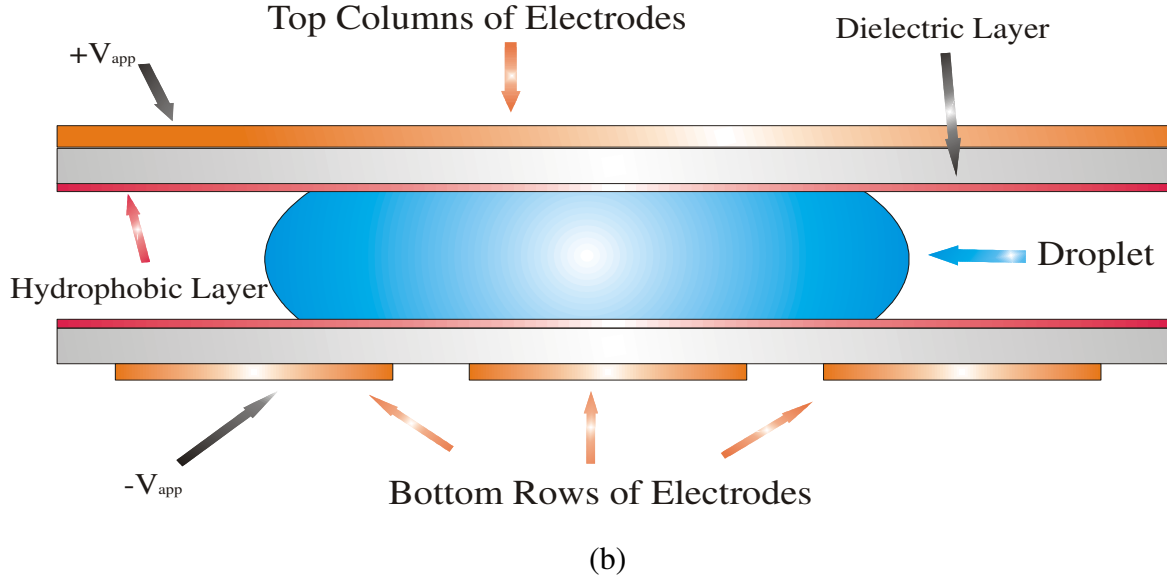
Figure 1.7 Schematic of a DMF multiplexer system is shown in this figure. (a) Top view and (b) cross-section of the proposed DMF multiplexer system.

The fundamental requirements for complete *m×n* addressability in a 2-D grid are met with threshold-based voltage actuation and enhanced localization of the electric field due to bi-polar voltage activation on a cross-referenced architecture. These two requirements are integrated into a DMF multiplexer system which will be elaborated upon in this thesis.

The threshold voltage phenomenon has been studied through a 2-D COMSOL simulation of a closed DMF system in Chapter 2, and the numerical results regarding this important effect are presented. To do this, two application modules of COMSOL, level-set and conductive media DC, have been used.

The electric field localization in a cross-referenced architecture, because of the bi-polar voltage activation, has been studied through a 3-D COMSOL simulation of the proposed DMF multiplexer structure in Chapter 3. The resulting electric field results show that the enhanced electric field at the intersection of the activated electrodes is greater than the electric field created in other regions.

A fabrication recipe for the proposed DMF multiplexer structure is shown in Chapter 4. The designed masks, photoresist type, baking times, dielectric and hydrophobic materials and spinner rates are reported. Moreover, the DMF multiplexer prototypes fabricated with this recipe are shown in this chapter.

The experimental setup used in this thesis is presented in Chapter 5. The high-resolution camera, *xyz* translation stage and micropipettes are shown.

The ultimate experimental results of the fabricated DMF multiplexer structures, with two microdroplets placed on the same electrode row, are shown in Chapter 6. The threshold voltage phenomenon has been studied experimentally, and the numerical results have been compared to these measurements.

Chapter 2

2.1 Threshold Voltage Phenomenon in a 2-D COMSOL Simulation

In this section a 2-D geometry of a closed digital microfluidic (DMF) system is modeled and simulated in COMSOL to meet the first requirement of the proposed DMF multiplexer system. According to the multiphysics nature of this problem, because of the effects of the electric fields on the surface tension and motion of the microdroplets, two different application modes of COMSOL (**level-set** and **conductive media DC)** have been used for this simulation. The two methods are presented in the next two subsections.

2.2 Level-Set Method

The first COMSOL application mode of interest is the level-set method for 2-D simulation of two-phase laminar flow. The level-set method tracks the interface of two immiscible liquids based on the difference of densities and viscosities of the two liquids (e.g., water and air). This new approach has been introduced by Osher [23] and Sethian [24]. In contrast to the other approaches that rely only on marking the boundary points, the level-set method takes the original curve and builds it into a surface.

2.2.1 Theory

In essence, the level-set method tracks the interface of two Navier-Stokes and level-set equations for incompressible fluids. For the closed DMF architecture of this research, the level-set method for two phase laminar flow solves the Navier-Stokes equation with surface tension introduced as the external force $F_{st}(x, y, t)$. Thus, the momentum and mass conservation yield

$$
\begin{aligned}
&\rho(x, y)\frac{\partial \bar{u}(x, y, t)}{\partial t} + \rho(x, y)\left(\bar{u}(x, y, t) \cdot \bar{\nabla}\right)\bar{u}(x, y, t) = \\
&\bar{\nabla} \cdot \left[-p(x, y)\bar{I} + \eta(x, y)\left(\bar{\nabla}u(x, y, t) + \bar{\nabla}u(x, y, t)^T\right)\right] + \vec{F}_{st}(x, y, t)
\end{aligned}
\tag{3}
$$

and

$$
\bar{\nabla} \cdot \bar{u}(x, y, t) = 0
\tag{4}
$$
,

where $\rho(x,y)$ is the fluid density, $u(x,y,t)$ is the velocity field, $\eta(x,y)$ is the dynamic viscosity and $p(x,y)$ is the pressure.

A volume fluid fraction ϕ is used to track the fluid positions, with $\phi = 0$ defined for fluid 1 regions and $\phi = 1$ defined for fluid 2 regions. There is a smooth transition of ϕ between fluid 1 and fluid 2 that is described by the following equation:

$$\frac{\partial \phi(x, y, t)}{\partial t} + \vec{u}(x, y, t) \cdot \bar{\nabla} \phi(x, y, t) =$$

$$\gamma \bar{\nabla} \cdot \left[\varepsilon \bar{\nabla} \phi(x, y, t) - \phi(x, y, t)(1 - \phi(x, y, t)) \frac{\bar{\nabla} \phi(x, y, t)}{\left| \bar{\nabla} \phi(x, y, t) \right|} \right] . \tag{5}$$

The parameters ε and γ are numerical values for discretizing the geometry [24-27]. Here, the fluid density and dynamic viscosity are functions of $\phi(x,y,t)$, so that

$$\rho(x, y) = \rho_1 + (\rho_2 - \rho_1)\phi(x, y, t) \tag{6}$$

and

$$\eta(x, y) = \eta_1 + (\eta_2 - \eta_1)\phi(x, y, t), \tag{7}$$

where ρ_1 and ρ_2 are the fluid densities of fluid 1 and fluid 2, respectively, and η_1 and η_2 are the dynamic viscosities of fluid 1 and fluid 2, respectively. These relations are then linked to the surface tension forces with

$$\bar{F}_{st}(x, y, t) = \bar{\nabla} \cdot \left[\sigma(x, y, t)(I - nn^T)\delta \right], \tag{8}$$

where δ is the Dirac delta function at the interface, and n is the unit vector normal to the boundary. The conductivity in this equation is then defined by

$$\sigma(x, y, t) = \sigma_1 + (\sigma_2 - \sigma_1)\phi(x, y, t), \tag{9}$$

with σ_1 and σ_2 as the conductivities of fluid 1 and fluid 2, respectively.

2.2.2 Material Settings

The conventional properties of water and oil are used in this simulation. The material properties can be selected from the COMSOL material library, or they can be entered manually. As shown in Figure 2.1, under the "Options" toolbox, the material properties and all other constant values of the simulation are entered. COMSOL saves each constant value by a specific name that is entered in the first column of the "Constants" window. These values have been used in the other parts of simulation using their predefined names.
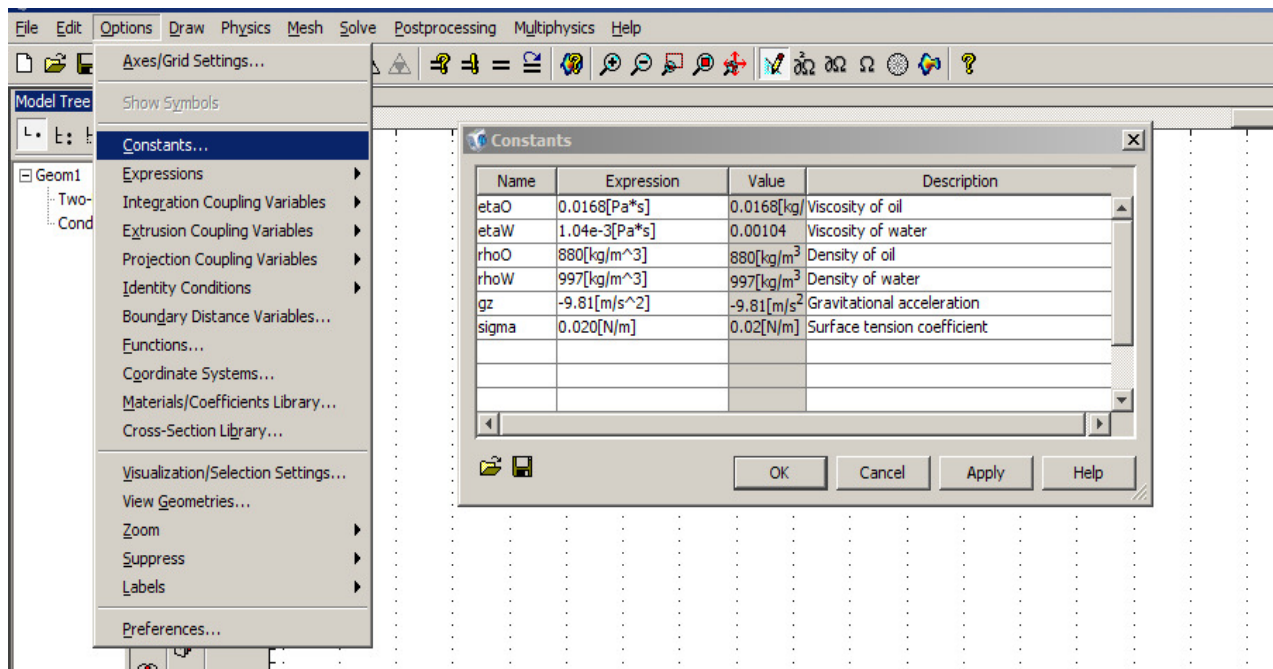
Figure 2.1 "Constants" windows Dialog box in COMSOL.

2.2.3 Boundary Settings

A 2-D cross-section of a closed DMF system is used for this simulation. As shown in Figure 2.2, a microdroplet is sandwiched between the top and bottom plates. The initial shape of the microdroplet is assumed to be axisymmetric with respect to the meridian plane.
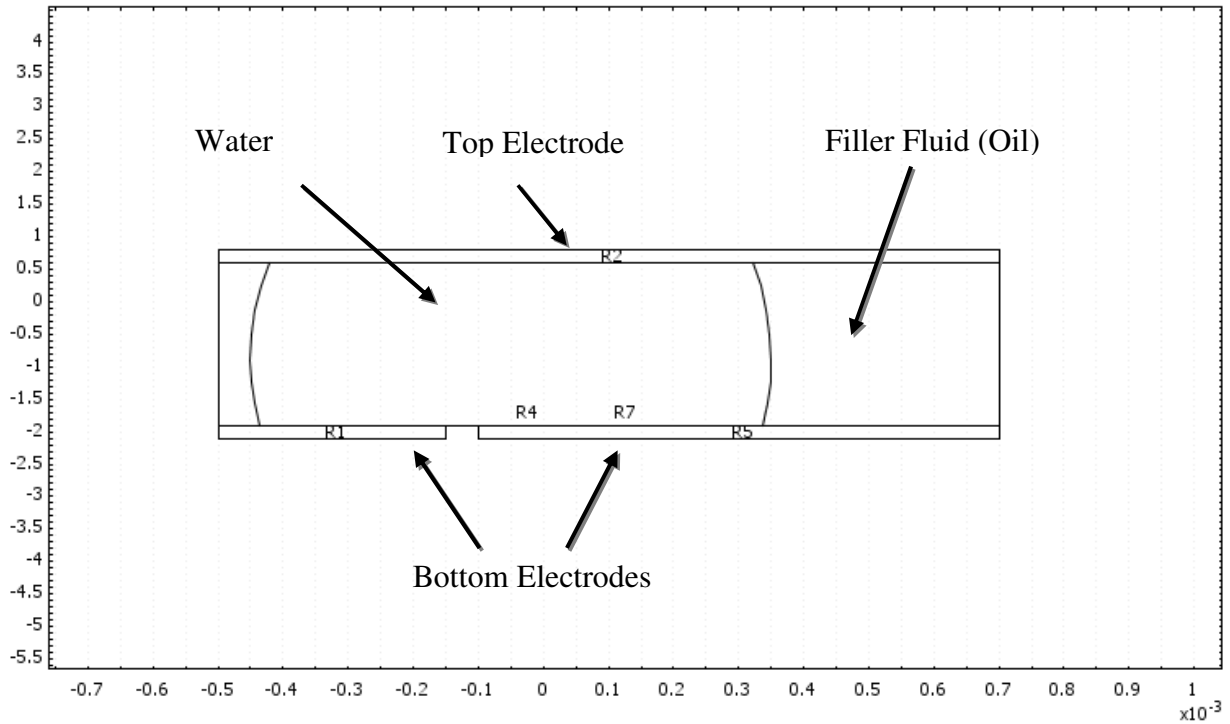
Figure 2.2 Geometry of the closed DMF system in COMSOL.

Level-set boundary conditions are shown in Figure 2.3. The green boundaries, which are top and bottom surfaces of the hydrophobic layers, are all chosen as wetted walls. The slip length is defined as the minimum mesh size of the geometry.

Boundary Settings - Two-Phase Flow, Laminar, Level Set (mmglf)

Equation

$\mathbf{n} \cdot \mathbf{u} = 0, \ \mathbf{t} \cdot [-p\mathbf{I} + \eta(\nabla\mathbf{u} + (\nabla\mathbf{u})^T)]\mathbf{n} = 0$

$\mathbf{F}_{fr} = -(\eta/\beta)\mathbf{u}, \ \mathbf{n} \cdot \mathbf{n}_{interface} = \cos(\theta)$

Boundaries | Groups

Boundary selection

Coefficients | Color/Style

Boundary conditions

Boundary type: Wall

Boundary condition: Wetted wall

Quantity	Value/Expression	Unit	Description
θ	theta	rad	Contact angle
β	5e-5	m	Slip length

Group:

☐ Select by group

☑ Interior boundaries

OK   Cancel   Apply   Help

Figure 2.3 Boundary settings of two-phase flow, laminar, level-set application modes.

Contact angles of the above wetted walls are then defined based on the Lipmann-Young equation that relates the applied voltage to the contact angle. All of the required equations for the contact angle and conductivity can be entered in the "Scalar Expressions…" toolbox that is shown in Figure 2.4.

15
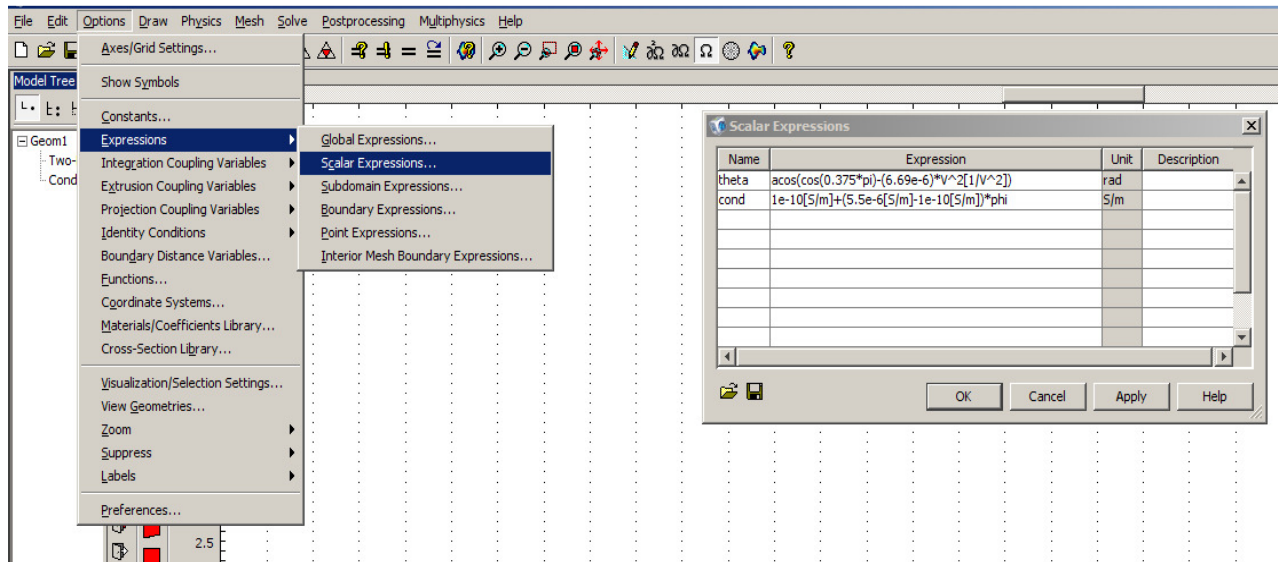
Figure 2.4 Contact angle and conductivity equations in the "Scalar Expressions…" window.

2.2.4 Subdomain Settings

As shown in Figure 2.5, pre-defined constant values in the material settings subsection are used for water and oil densities and dynamic viscosities.

Only two out of six available subdomains are active subdomains (water microdroplet and oil) in the level-set application mode, because other subdomains are related to the underlying and overlying electrodes that are not considered in the level-set application mode. The most important thing that should be taken into consideration is the relative permittivity of the "Microfluidic" tab in the subdomain settings window. Similar to the density, dynamic viscosity and conductivity, the relative permittivity of the domain can be defined as a function of the level-set function "φ" to simplify the numerical calculations. This relationship is shown in the windows dialog box shown in Figure 2.6.
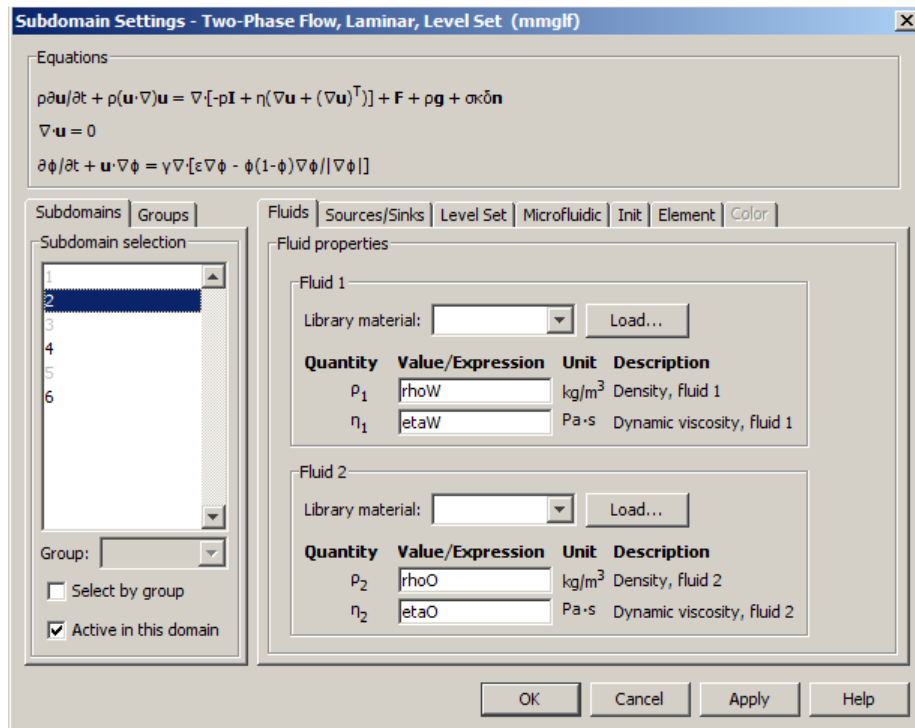
Figure 2.5 Subdomain settings of two-phase flow, laminar, level-set application mode.

Subdomain Settings - Two-Phase Flow, Laminar, Level Set (mmglf)

Equations

$$\rho\partial\mathbf{u}/\partial t + \rho(\mathbf{u}\cdot\nabla)\mathbf{u} = \nabla\cdot[-p\mathbf{I} + \eta(\nabla\mathbf{u} + (\nabla\mathbf{u})^T)] + \mathbf{F} + \rho\mathbf{g} + \sigma\kappa\delta\mathbf{n}$$

$$\nabla\cdot\mathbf{u} = 0$$

$$\partial\phi/\partial t + \mathbf{u}\cdot\nabla\phi = \gamma\nabla\cdot[\epsilon\nabla\phi - \phi(1-\phi)\nabla\phi/|\nabla\phi|]$$

Subdomains | Groups

Fluids | Sources/Sinks | Level Set | Microfluidic | Init | Element | Color

Subdomain selection

1
2
3
4
5
6

Group:

☐ Select by group

☑ Active in this domain

Physics settings for microfluidics

Quantity	Value/Expression	Unit	Description
ϵ_r	80+(2.2-80)*phi		Relative permittivity
λ_{mfp}	1e-6	m	Mean free path

OK   Cancel   Apply   Help

Figure 2.6 Relative permittivity in the subdomain settings of level-set mode is defined based on the level-set function.

2.3   Conductive Media DC

The second COMSOL application mode used in this simulation is the conductive media DC. This application mode is used to calculate the distributed voltage and electric field inside the microdroplet. The calculated voltage will then be used in finding the contact angle of the microdroplet on the hydrophobic surface.

2.3.1 Theory

The conductivities of the level-set method enter into the analysis through the quasi-static fields, conduction currents $J^e(x,y,t)$ and potential distribution $V(x,y,t)$ of Poisson's equation:

$$\bar{\nabla}\left(\sigma\left(x,y,t\right)\bar{\nabla}V\left(x,y,t\right)-J^e\left(x,y,t\right)\right)=0 \,. \tag{10}$$

The multiphysics response of the system is quantified by defining the contact angle θ with the Lippmann-Young equation:

$$\cos\theta=\cos\theta_0+\frac{C}{2\gamma_{LV}}V_{diff}^2 \quad, \tag{11}$$

where θ_0 is the initial contact angle without the applied voltage, C is the capacitance per unit area, and γ_{LV} is the liquid-vapor surface tension. The above equation is the key part of the multiphysics nature in this simulation. By using the Lippmann-Young equation, the calculated voltage at the boundaries of the medium is used to find the contact angle of the microdroplet on the hydrophobic surface in the DMF system.

2.3.2 Boundary Settings

The boundary settings of the second application mode, conductive media DC, are shown in Figure 2.7. The green and red boundary lines define the activated underlying electrode in the closed DMF system, while the other electrodes are grounded.
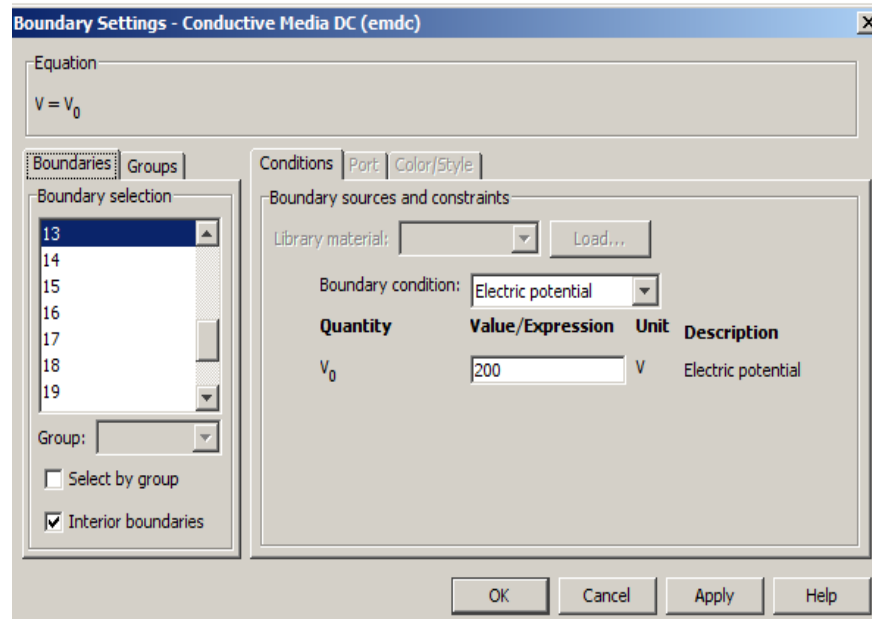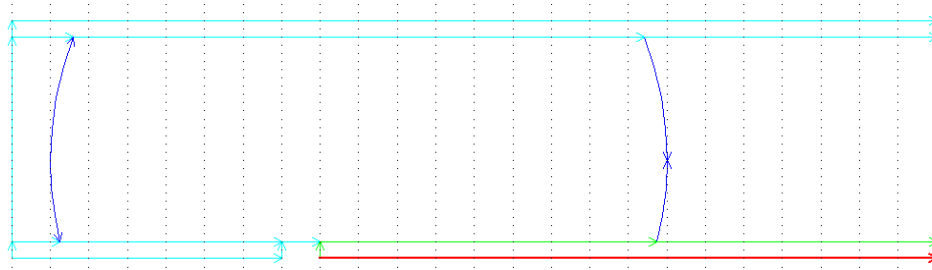
Figure 2.7 Boundary settings of the conductive media DC application mode are shown in this figure. A voltage of 200 V is applied to the right bottom electrode and the other electrodes are grounded.

2.3.3 Subdomain Settings

As shown in Figure 2.8, pre-defined materials such as copper and PDMS (as the dielectric layer) are selected from the COMSOL material library.
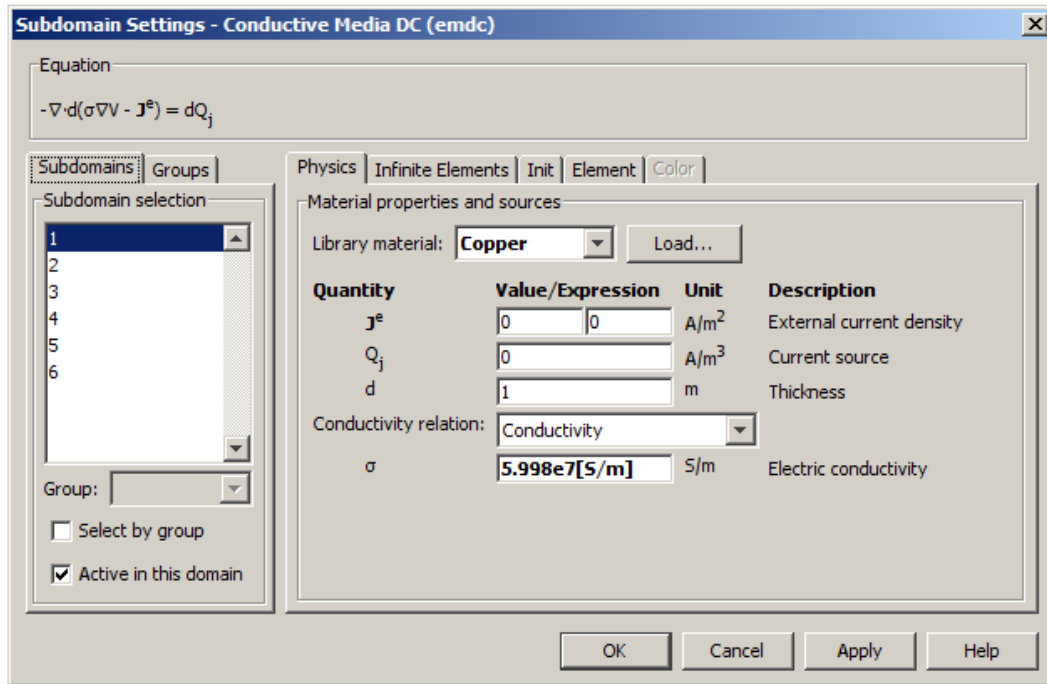
Figure 2.8 Subdomain settings of the conductive media DC application mode.

2.4   Solve the Problem

In this step of the simulation, both application modes have been selected to solve the problem in the multiphysics situation. Conductive media DC application mode is straightforward, but the level-set method can be challenging mainly because of its initialization. Before running the simulation in a transient type, the level-set function should be initialized. To do this, in the "Solver Parameter" windows dialog box, the "Transient initialization" option under the "Analysis types" tab and also the "Direct UMFPACK" under the "Linear System Solver" tab have been selected to run the simulation for the specified time duration and then store the final solution of this transient initialization analysis. In order to store the initial solution of the simulation, the "Solver Manager…" option under the "Solve" toolbox can be used. This stored solution can then be used as the initial point for the "Transient" analysis of the system. As shown in Figures 2.9 (a-c), after selecting the desired solver and simulation analysis type and clicking on the "Run" button, the acquired results have been stored and used as the initial point for the transient analysis of the simulated closed DMF system.
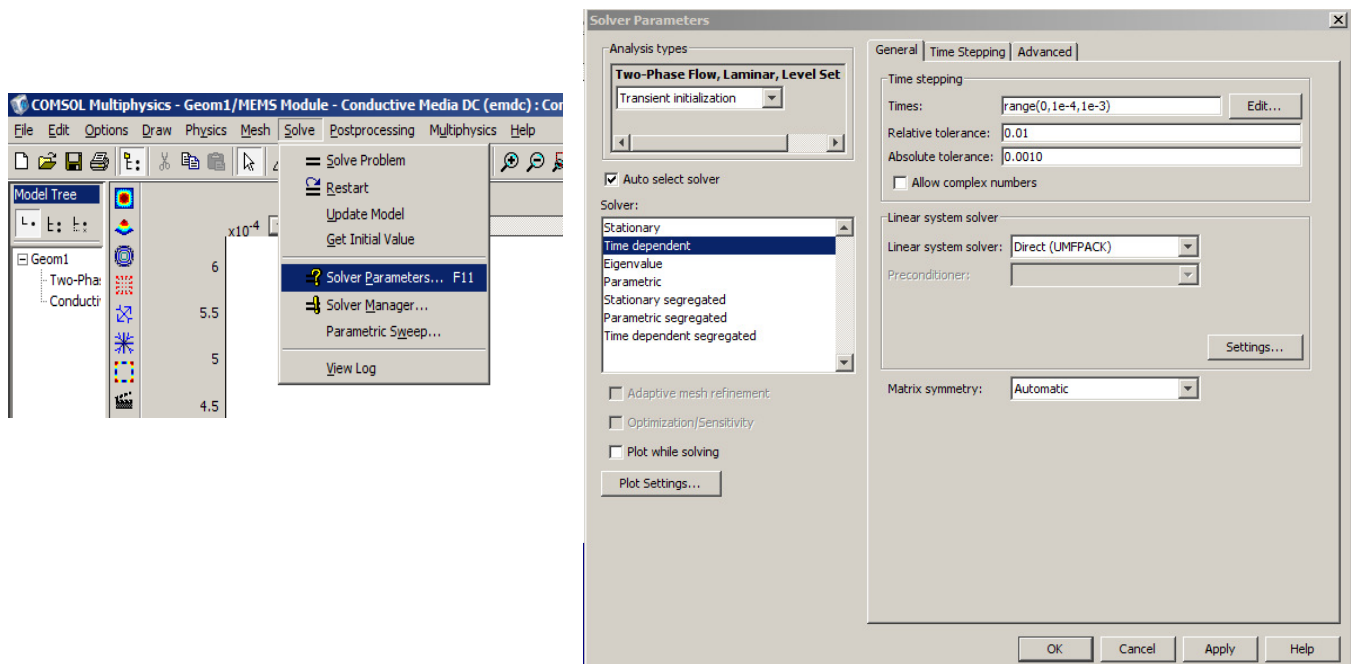
(a)
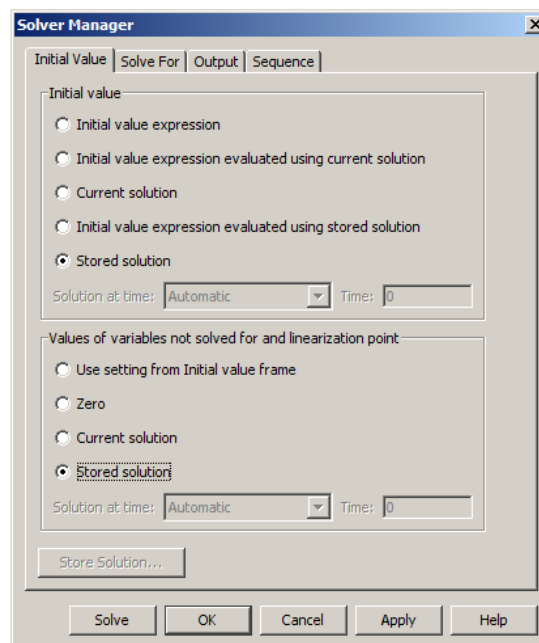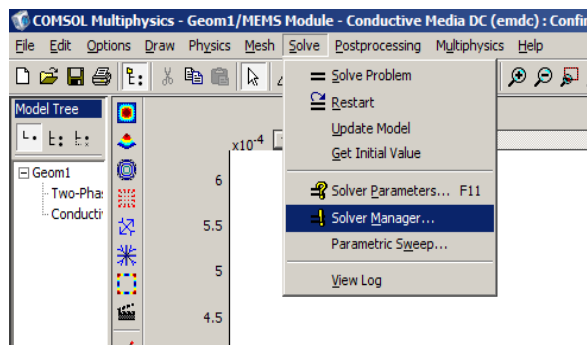
(b)
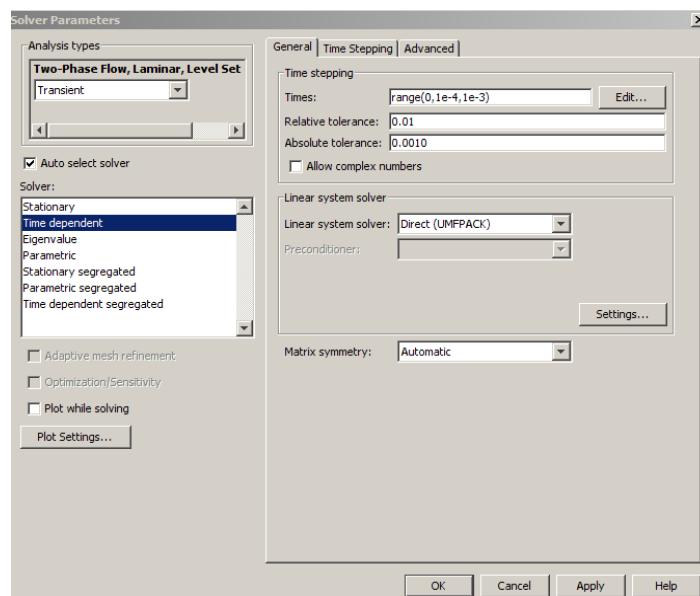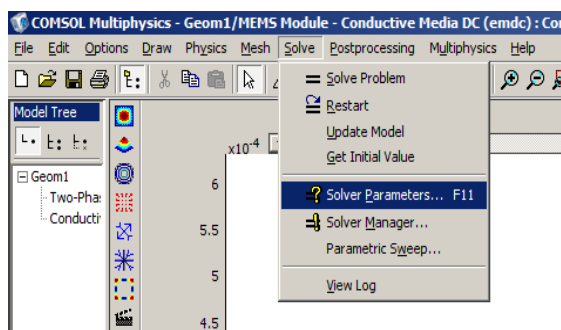
(c)

Figure 2.9 Solving procedure of the level-set application mode is shown in this figure: (a) Transient initialization analysis type and Direct UMFPACK have been selected, and the problem is solved, (b) results have been stored to be used as the initial point for the transient analysis type of the problem, and (c) Transient analysis type has been selected to solve the problem.

23

2.5   Results

After finishing the modeling part of a 2-D closed DMF system in COMSOL, the significance of the threshold voltage phenomenon has been studied. In this section, the numerical results of the simulation for different applied voltages have been shown. These numerical analyses will be verified by experimental results in Chapter 6.

In order to study the threshold voltage phenomenon, the problem has been solved for a variety of applied voltages to find the exact voltage in which the microdroplet starts to move. The range of the applied voltage can be divided into three parts: lower than the threshold voltage, at the threshold voltage and greater than the threshold voltage. In the first part (i.e. $V_{app} < V_{th}$) the microdroplet contact angle change is very small, and the microdroplet does not start to move due to the lack of sufficiently large EWOD forces. In the second part (i.e. $V_{app} = V_{th}$) there is a noticeable change in contact angle, and the microdroplet starts to move towards the activated electrode. In the third part (i.e. $V_{app} > V_{th}$), after passing the threshold voltage, the contact angle change increases considerably and the microdroplet moves faster. These numerical results are shown in Figures 2.10-12.
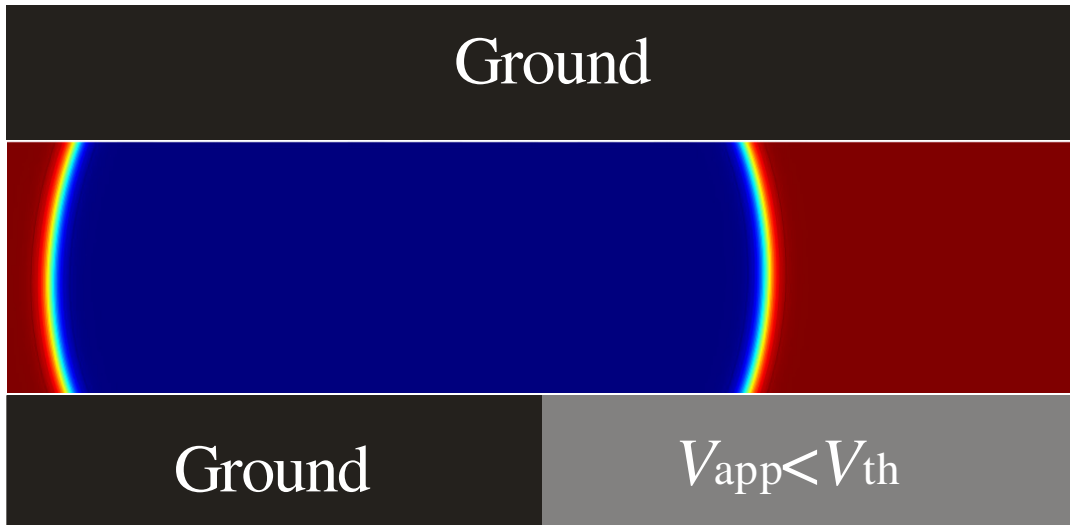
Figure 2.10 COMSOL result of a 2-D closed DMF system before the threshold voltage, $V_{app}<V_{th}$.

Figure 2.10 shows the droplet with negligible actuation for $V_{app} < V_{th}$. The contact angle change becomes apparent in Figure 2.11, where $V_{app} = V_{th}$. Here, the threshold voltage initiates the contact angle change of the right edge of the microdroplet. The change becomes noticeable, compared to the previous case, and surface tension forces are large enough to initiate the microdroplet motion. The contact angle change of the microdroplet at the voltages beyond the threshold voltage is shown in Figure 2.12.
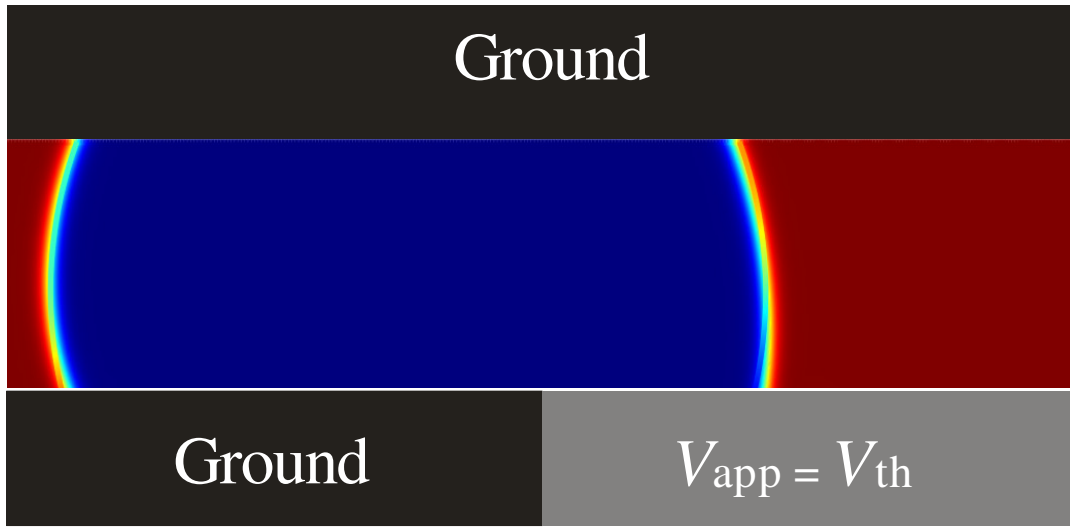
Figure 2.11 COMSOL result of a 2-D closed DMF system at the threshold voltage, $V_{app}=V_{th}$.
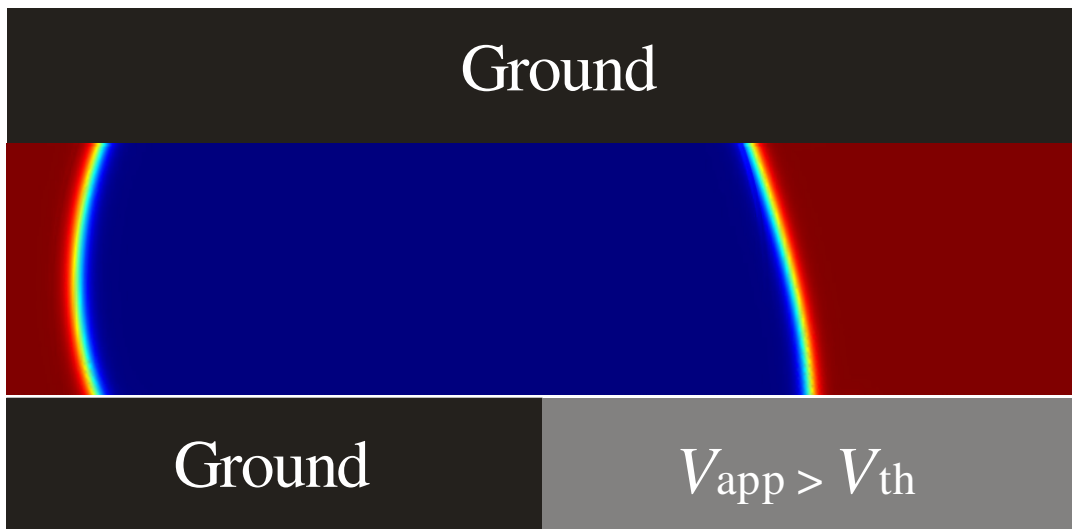
Figure 2.12 COMSOL result of a 2-D closed DMF system after the threshold voltage, $V_{app}>V_{th}$.

2.6   Conclusions

The threshold voltage phenomenon is the result of hysteresis effects in DMF systems. If the surface was devoid of hysteresis, the microdroplet would immediately start to move as soon as the adjacent electrode was actuated [21, 28]. However, there is an electric potential threshold below which the microdroplet does not move (i.e., there is a pseudo-gradient of wettability below which the microdroplet cannot move). The hysteresis effect is the deviation of the contact angle from its theoretical value due to physical effects such as microscopic surface roughness and defects.

Moreover, the threshold voltage magnitude depends on various parameters: the microdroplet liquid material, hydrophobic surface material, dielectric material and thickness, gap size between the adjacent electrodes and microdroplet size. For example, smaller microdroplet and gap sizes between the neighboring electrodes and thinner dielectric layers can decrease the threshold voltage of the system. So, in order to use the proposed DMF multiplexing format in a cross-referencing DMF system, the fabricated prototypes must be characterized, and the threshold electric potential must be measured for the desired microdroplet. Then, the applied voltages to the electrodes are selected based on the measured threshold voltage.

It is worthy to note that the threshold voltage phenomenon is an undesirable effect for most researchers working on DMF devices, due to its destructive effects on biological samples [19]. Many efforts have been made in this field to reduce the threshold voltage in the DMF prototypes. However, this research has taken advantage of this seemingly unfavorable phenomenon to enhance the addressability and localization of the DMF systems.

Chapter 3

3.1   3-D COMSOL Simulation of a DMF Multiplexer

In this section, the second requirement of the proposed DMF multiplexer, which is localization of enhanced electric field due to bi-polar voltage activation, has been studied numerically. A 3-D model of the proposed DMF multiplexer is developed in COMSOL to study the localization of the electric field at the intersection of the activated electrodes.

3.2   Bi-Polar Voltage Activation Protocol

One of the main features of the proposed DMF multiplexer, compared to the conventional cross-referencing system, is the bi-polar voltage activation (+*V*, -*V*). By combining this bi-polar voltage activation scheme and the threshold-based voltage actuation many of the complexities of the conventional cross-referencing system can be resolved.

3.3   3-D Simulation of Localized Electric Field in a Multiplexer

In order to study the effect of the proposed bi-polar voltage activation scheme, a 3-D simulation of a DMF multiplexer system based on the bi-polar scheme has been carried out using COMSOL. This simulation has only one electrostatic component, and similar to the electrostatic part of the 2-D closed DMF system, the conductive media DC application mode of COMSOL is used. The boundary conditions of this simulation are selected in a way that only the second top ($m = 2$) and bottom ($n = 2$) electrodes experience electric potentials of $+V_{app}$ and $-V_{app}$, respectively. In this simulation the applied voltage to the bottom and top electrodes are selected by considering the threshold voltage of the DMF system described in Chapter 2. The isolated V_{app} would be smaller than the threshold voltage V_{th}, while $2V_{app}$ is greater than V_{th}.

An isotropic view of the final result of this 3-D DMF multiplexer simulation is shown in Figure 3.1. It is noted that the magnitude of the electric field at the intersection of the second top and bottom electrodes are noticeably higher than that in the other regions of the DMF multiplexer.
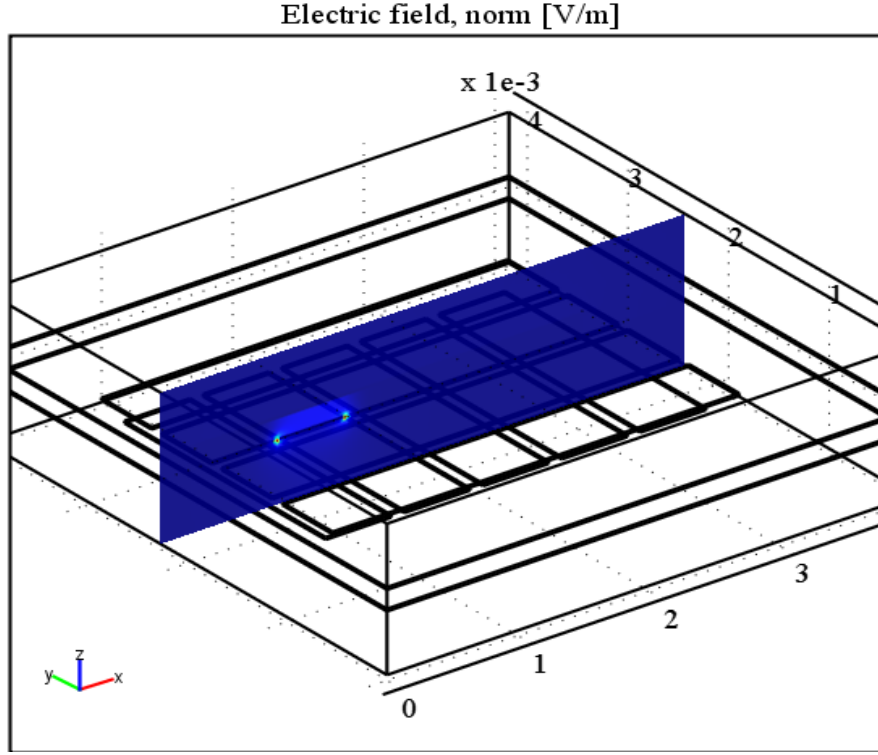
Figure 3.1 Isotropic view of the resulting electric field along the activated electrode in the DMF multiplexer system.

As shown in Figure 3.2, the resulting normalized electric field at the intersection of the two activated electrodes is higher than the threshold electric field created by the threshold voltage, V_{th}, required for initiating the motion of the microdroplet. However, the resulting electric fields in the other isolating regions (e.g., $m = 2$ and $n = 3$) are below the threshold electric field and cannot initiate the microdroplet motion. Given microdroplets placed in the same row (i.e. $m = 3$), only the one at the position $m = 2$ and $n = 2$ will move to the left.
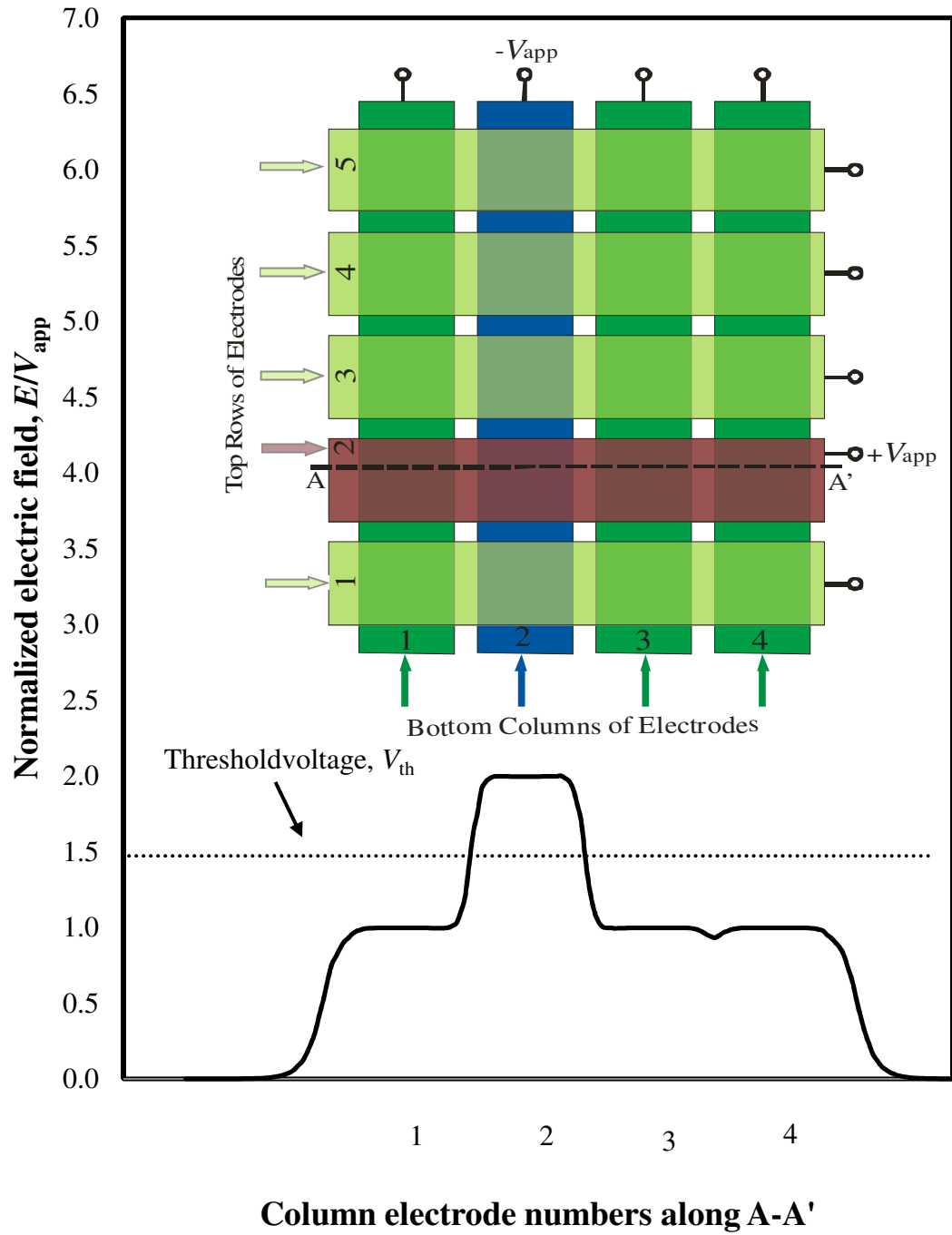
Figure 3.2 Resulting electric field of a 3-D DMF multiplexer system simulation in COMSOL is shown.

3.4   Conclusions

Based on the COMSOL results of this chapter (and shown in Figure 3.3), the localized electric field at the intersection of the activated top and bottom electrodes is greater than the electric field elsewhere. It is therefore large enough to initiate motion of the microdroplet placed on a cell adjacent to the destination cell. The electric fields created in other regions of the activated electrodes experiencing $+V_{app}$ are not enough to move a droplet. The principle of $m \times n$ addressability should therefore be possible with this proposed multiplexer.

Some practical comments can also be made on the operation of the proposed structure. From the electric field distribution along the activated top electrode, it can be seen that the electric field decreases slightly in the gaps between the neighboring electrodes. Thus, smaller gaps would be desirable to reduce this fringing effect.

AS well, in some bio-applications small localizations are required. For this goal, narrower electrodes can be designed and fabricated. Then, as needed, electrode groupings can be used to actuate large-scale microdroplets in the system.
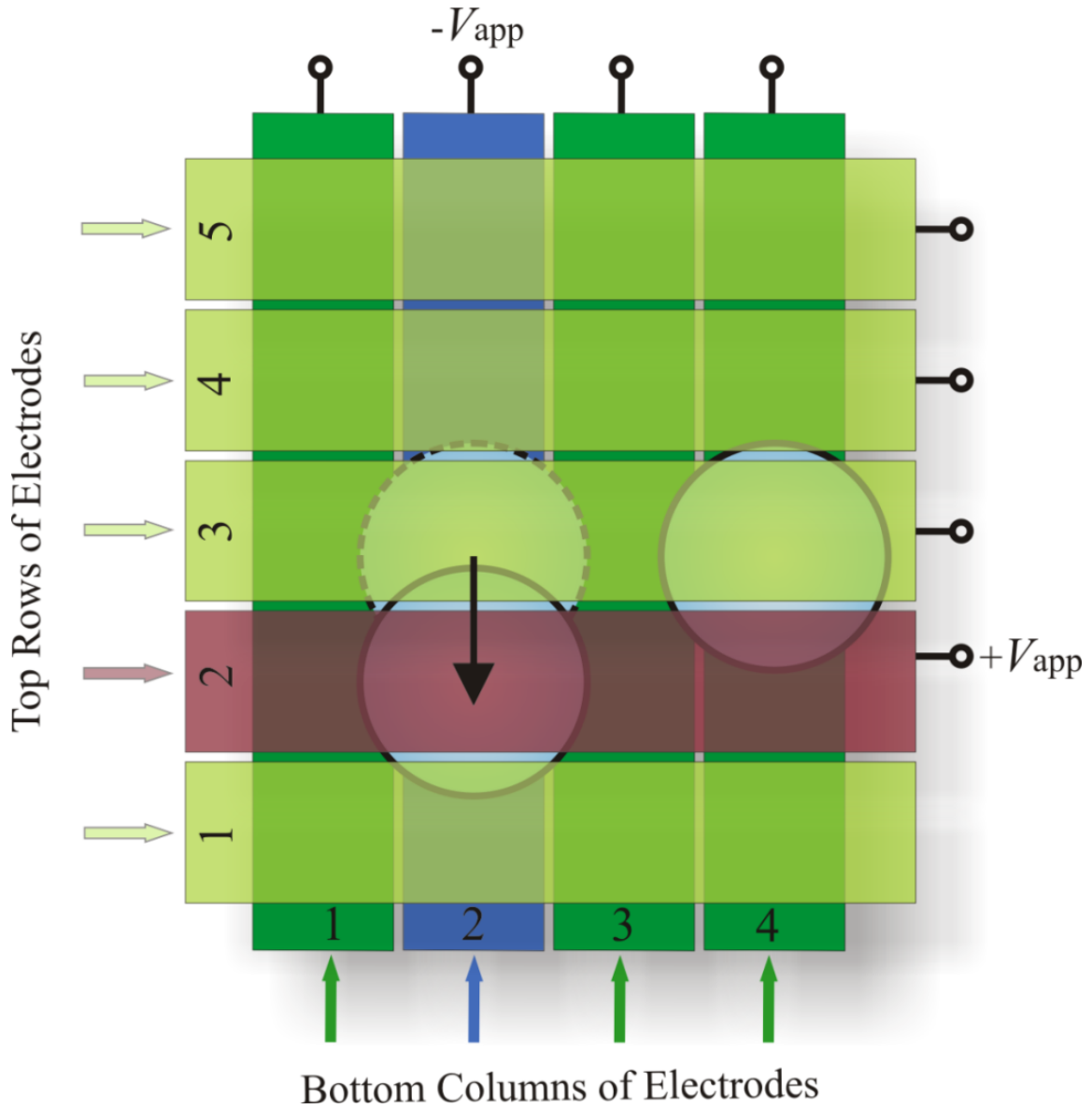
Figure 3.3 Enhanced electric field at $m = 2$, $n = 2$ intersection causes the motion of the left microdroplet to the bottom cell, while the right microdroplet experiencing $+V_{app} < V_{th}$ does not move.

Chapter 4

4.1 Fabrication of a Multiplexer System

In this chapter, the DMF multiplexer fabrication is presented. The general arrangement of these steps has been defined previously [29, 30]. The details of each step are characterized for use in any new DMF design. For this purpose, different time intervals, speeds, and curing temperatures have been tested to find the best recipe for the DMF multiplexer prototype.

4.2 Mask Designs

The first step of transferring a pattern onto a metal coated substrate involves designing a mask with the desired pattern. For this goal different software packages like AutoCAD and CorelDRAW can be used. In order to design a mask for a DMF system, numerous aspects should be taken into consideration. These aspects include the size limitation, etching method, and photoresist type.

Size limitation: The number of electrodes and address lines can be defined according to the available space on the DMF system. The conventional addressing of the inner square electrodes in this aspect may present limitations for gap sizes between adjacent electrodes.

Etching method: The design of the mask can be different for different etching methods (i.e. wet or dry etching). For example, because of undercutting in wet etching, there are often limitations for the size of the electrodes and the gaps between them. Dry etching methods are less susceptible to this limitation, and smaller electrodes with small gaps are achievable.

Elaborated in Chapter 1, the main motivation of the cross-referencing architecture is enhanced addressability. As shown in Figure 4.1, the greater the number of inner electrodes, the larger the size of the open or closed DMF prototype. As a result, electrical connectivity to the inner electrodes becomes a challenge. More precisely, the address lines of these inner electrodes, which must be placed between electrodes, can result in shorting, overlapping and crossing of each other when the design is scaled up. This leads to a lower limit for the gap size *D,* defined in Figure 4.1 (b).
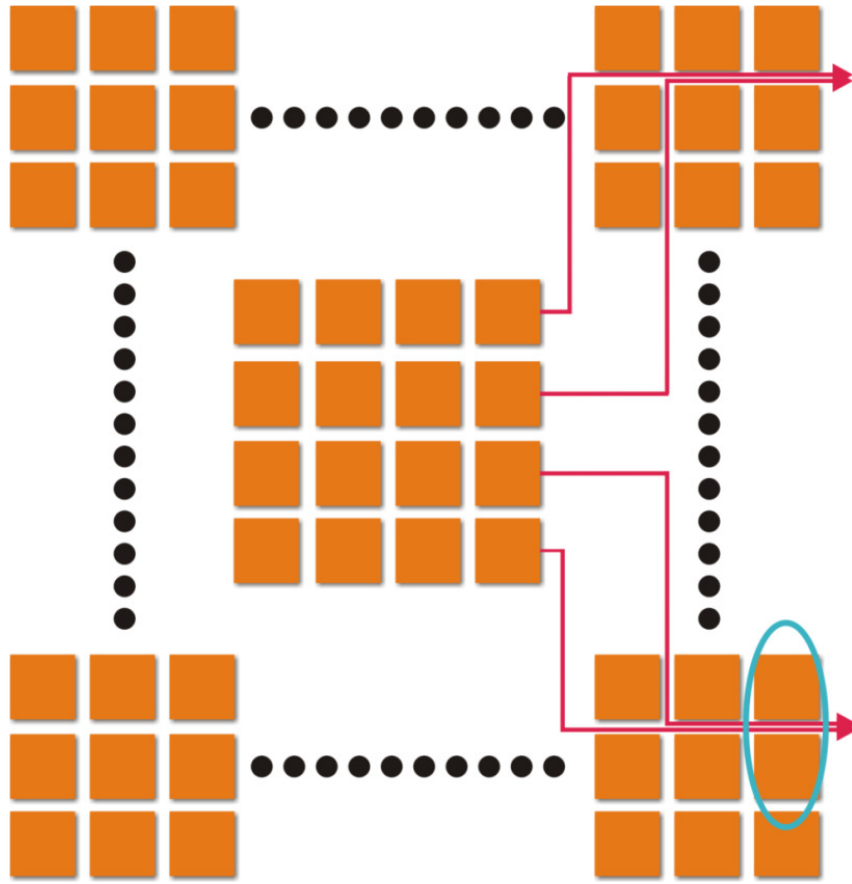
(a)
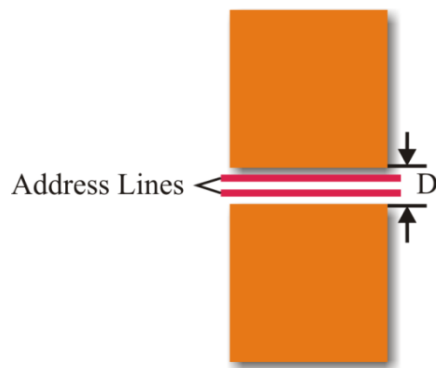
(b)

Figure 4.1 Addressability issues are shown for open and closed DMF systems. (a) Schematic of an open or a closed DMF system with a large number of inner electrodes. (b) Gap size, D, limitation because of the inner address lines between the electrodes.

To overcome the addressing challenges of the inner electrodes, Fan et. al. [1] proposed the cross-referencing DMF system. In this system, two arrays of electrodes are placed orthogonally, and the liquid microdroplet is sandwiched between them (Figure 4.2). In order to move the microdroplet to the destination cell, one of the intersecting electrodes at the destination cell is grounded and the other one is activated by a voltage +V.
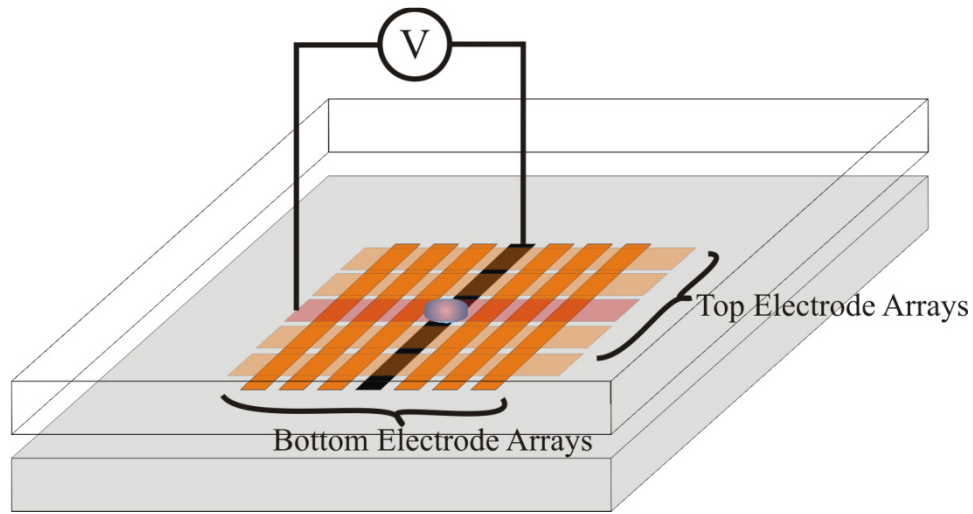
(a)
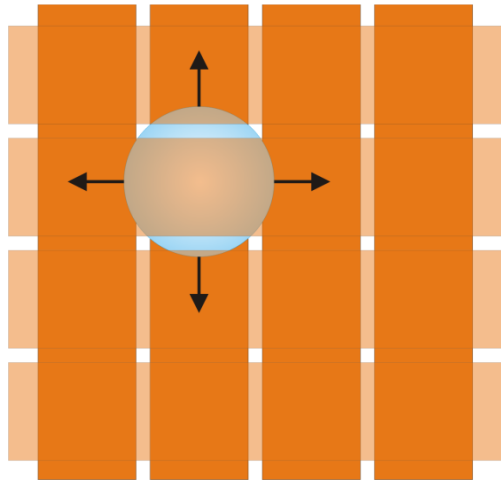
(b)

Figure 4.2 The cross-referencing structure is shown in this figure. (a) An isotropic view of the conventional cross-referencing structure is presented. (b) Top view of the proposed cross-referencing system by Fan et. al.

Pre-coated copper (45 nm thickness) microscope slides (EMF corporation, Ithaca, NY) have been used as the substrate of the proposed DMF multiplexer system. All masks designed in this research are limited to the size of a microscope slide with the DMF multiplexer structure defined by arrays of *X* and *Y* electrodes. These arrays are designed with CorelDRAW and are shown in Figures 4.3 (a-d). Different electrode sizes and gap distances between adjacent electrodes have been used in the designs. The electrode pads are placed far from the main electrodes, because the electric field created by these pads at higher voltages can affect the motion of microdroplets. Also, the top electrode plate is placed orthogonally at the middle of the bottom plate, so there should be sufficient room on the bottom plate for plate spacers.

(a)

(c)

(b)

(d)
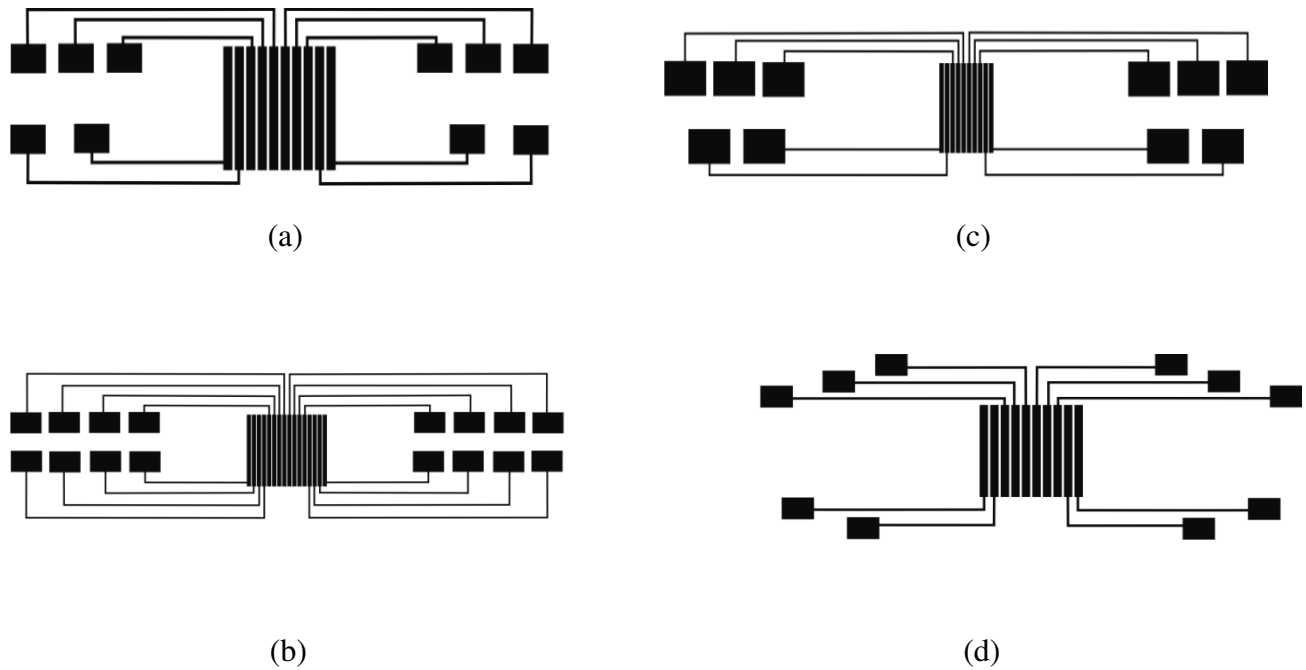
Figure 4.3 Various DMF multiplexer masks are presented in this figure. (a) Number of electrodes = 10, electrode size = 1 mm, gap size = 250 µm. (b) Number of electrodes = 16, electrode size = 500 µm, gap size = 100 µm. (c) Number of electrodes = 10, electrode size = 500 µm, gap size = 100 µm. (d) Number of electrodes = 10, electrode size = 1 mm, gap size = 250 µm.

Depending on the accuracy and the resolution of the masks, the masks can be printed on a transparency film or a glass plate. Because the smallest feature size of the above designed masks is 100 μm, the masks have been printed on transparency films. For smaller feature dimensions (e.g. 50 μm or smaller), the mask should be printed on a fused silica or quartz plate with a mask pattern generator.

4.3   Fabrication Recipe

After finishing the mask design of the DMF multiplexer arrays, the next step involves fabrication. In each step of the fabrication recipe, different variables such as spinning time, spinning velocity, curing time and developer solution ratio must be characterized. The optimal recipe is presented here.

4.3.1 Photoresist

Photoresist is a UV light-sensitive polymer that can be used as a pattern protector on a metal-coated substrate. Photoresist has a developer solution which washes away the sensitized areas of the cured photoresist on the substrate. It can be positive or negative. As shown in Figure 4.4, the UV exposed areas of the positive photoresist will be washed in the developer solution.

Figure 4.4 Positive Photoresist

In the case of negative photoresist, the UV exposed areas of the negative photoresist will remain after developing (Figure 4.5).

Figure 4.5 Negative Photoresist

For the fabrication work presented here, the positive photoresist PHOTOPOSIT SP 24D is used.

4.3.2 Spinner

For a uniform photoresist layer on the pre-coated copper microscope slides WS-650SZ-6NPP/LITE spinner is used. A microscope slide mount is attached to the spinner. For cleaning the interior, a nitrogen purge line is used. Mounting of slides is achieved with a vacuum chuck.
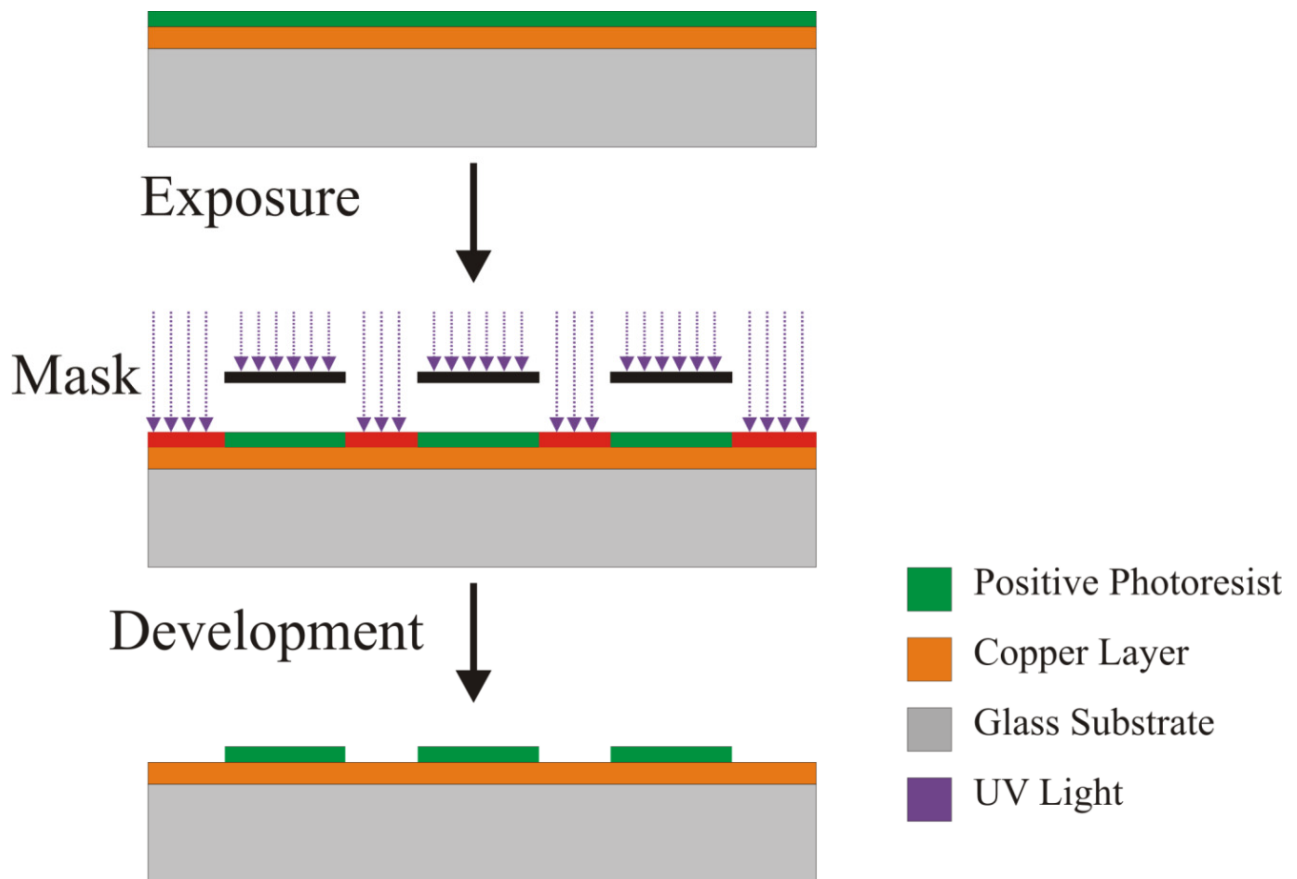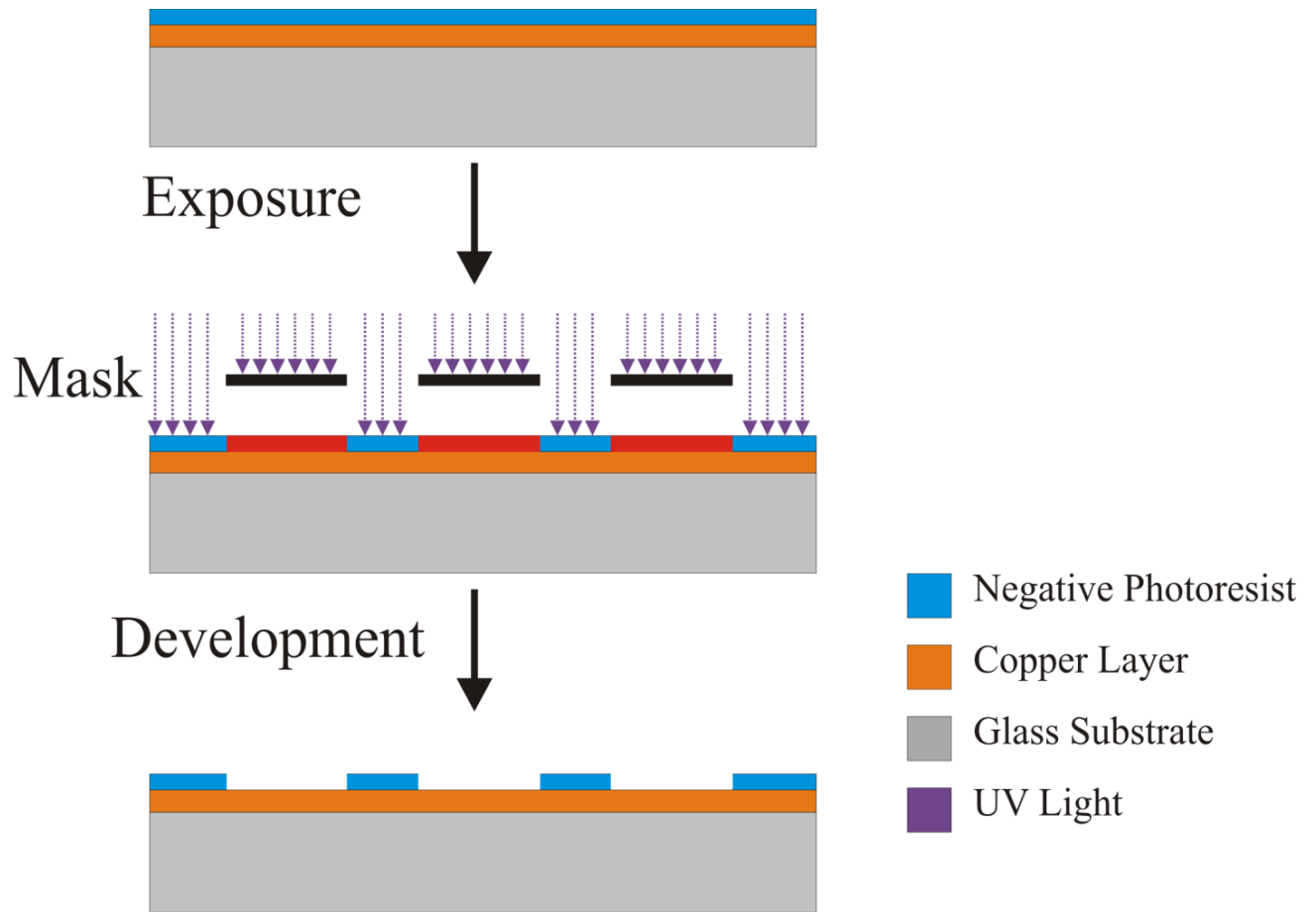
After setting numerous pre-coated copper microscope slides on the spinner, different velocities from 1000-5000 rpm and spinning times from 20 (s) - 90 (s) have been tried. Finally a 60 seconds spinning period at 5000 rpm was chosen as the best spinning time and velocity.

4.3.3 UV Exposure Light

After spinning the photoresist on the pre-coated copper microscope slides, the photoresist layer is baked in an oven at 90 ℃. After one hour, the liquid photoresist layer is solid.

The next step involves transferring the desired pattern to the photoresist layer. To do this, UV exposure light is applied to the photoresist layer through the designed mask. For this goal, a 250 nm short wave UV light is used. Samples are exposed to the UV light for 15 minutes.

4.3.4 Photoresist Development

After applying UV to the positive photoresist surface, the areas that are not covered with the designed mask will be sensitized. These sensitized areas will then be washed away by the photoresist developer solution. PHOTOPOSIT SP 24D photoresist is prepared in an aqueous solution of 0.8 % by weight (0.2 N) sodium hydroxide in DI water. The developer solution temperature should be kept between 29-35℃ (84-95°F). The mixing ratio of the developer solution to DI water is 1 to 7.

4.3.5 Etching

There are two different etching methods: dry and wet. For higher resolution and better accuracy, dry etching methods like deep reactive ion etching (DRIE) can be used, while for larger dimensions wet etching methods are preferred. Wet etching methods are less expensive and faster, and are therefore employed here for these large-scale (greater than 50 µm) features. On these scales undercutting is minimal.

The next step in the DMF multiplexer fabrication procedure involves wet etching the pre-coated copper microscope slides, which are now covered with the patterned photoresist layer. After putting these samples into the etchant, the areas of the copper that are protected by the patterned photoresist will be remain, while the uncovered areas will be washed away by the etchant.

In this fabrication recipe, Ferric Chloride is used as the copper etchant. Samples are submerged into ferric chloride solution for 20 seconds and quickly rinsed.

4.3.6 Photoresist Removal

After etching the copper-coated microscope slides, the designed pattern is transferred to the copper layer. The next step of the fabrication involves removing the patterned photoresist on the etched copper layer. To do this a photoresist thinner solution is used.

PHOTOPOSIT SP 24D photoresist is stripped in an aqueous solution of 1.4-1.8 % by weight (0.35-0.45 N) sodium hydroxide in DI water at 45-55℃ (113-131℉) after 1 minute. The removed photoresist will dissolve in this caustic solution. An additional of 1-4 ml per gallon of Antifoam 2750 may be used to control foaming.

4.3.7 Dielectric and Hydrophobic Layers

Conventional DMF systems use a thin Parylene C layer and a Teflon layer as the dielectric and the hydrophobic layers, respectively. Recently, DMF systems with a polydimethylsiloxane (PDMS) layer have also been reported [29-31]. PDMS can act as both the hydrophobic and dielectric layers and is, therefore, easier to fabricate.

To make the PDMS solution, silicone elastomer cure agent and silicone elastomer base should be mixed with the ratio of 1 to 10. The PDMS solution is then spin-coated onto the patterned copper-coated substrate with the WS-650SZ-6NPP/LITE spinner using the same velocity and time as the photoresist (velocity = 5000 rpm, time = 60 s).

After spinning the PDMS layer on the patterned copper microscope slide, it is cured. To do this, the covered copper microscope slide with the PDMS layer is placed into an oven at 150℃. After 24 hours, the PDMS layer is completely cured and is ready to be used.

While PDMS offers simple fabrication, compared to multilayer structure, it does have one disadvantage. The required threshold voltage is large. With this in mind, solutions are proposed here to reduce the applied voltage on the DMF multiplexer prototype:

1. Smaller gap sizes are used between the adjacent electrodes in the designed mask to allow for smaller microdroplet sizes and reduced applied voltages.
2. A Teflon layer on the PDMS layer can be used to provide easier motion between the top and bottom electrode plates [31].

With these solutions, the DMF system threshold voltage can be reduced well below 200 V.

4.4 Fabricated Multiplexer Structures

The process times, spinning velocities, developer mixing ratios and photoresist baking times are shown in Table 1.

Table 4.1 Fabrication recipe of the DMF multiplexer structures

Fabrication Recipe		
Step No.	**Step Description**	**Features**
1	Positive photoresist spinning	5000 (rpm), 60 (s)
2	Baking the covered copper microscope slides with the positive photoresist layer	1 (hr), 90 (℃)
3	Applying 250 nm short wave UV light	15 (min)
4	Developing the exposed photoresist layer on the copper microscope slides	3 (min)
5	Etching the developed samples	10 (s)
6	Removing the photoresist layer by putting the etched samples into the photoresist thinner solution	60 (s)
7	Spinning the PDMS layer on the patterned copper microscope slides	5000 (rpm), 60 (s)
8	Baking the covered copper microscope slides with the PDMS layer	24 (hr), 150 (℃)

Two examples of electrode arrays fabricated, using the above fabrication recipe, are shown in Figures 4.6 and 4.7. To have a fixed gap size between the top and bottom electrode plates, two 250 μm spacers are used at opposite ends of the top and bottom plates.

The final DMF multiplexer structure is shown in Figure 4.8. The *X* electrodes are placed on top of the *Y* electrodes with a constant gap size of 250 µm.
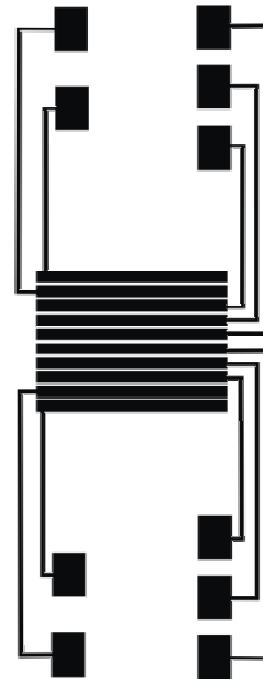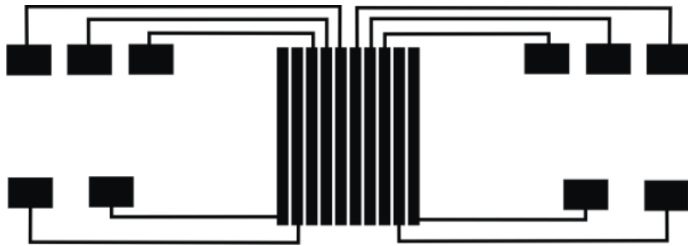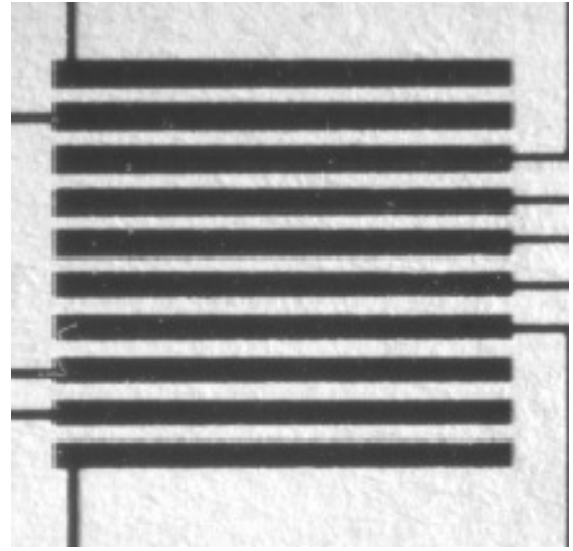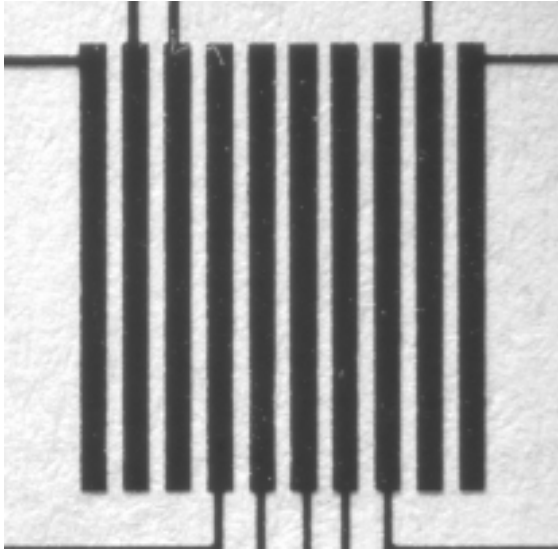
(a)

(b)

Figure 4.6 Fabricated *X* and *Y* electrodes are shown in this figure. (a) *X* electrodes, Number of electrodes = 10, electrode size = 1 mm, gap size = 250 µm. (b) *Y* electrodes, Number of electrodes = 10, electrode size = 1 mm, gap size = 250 µm.

Pre-coated copper microscope slide
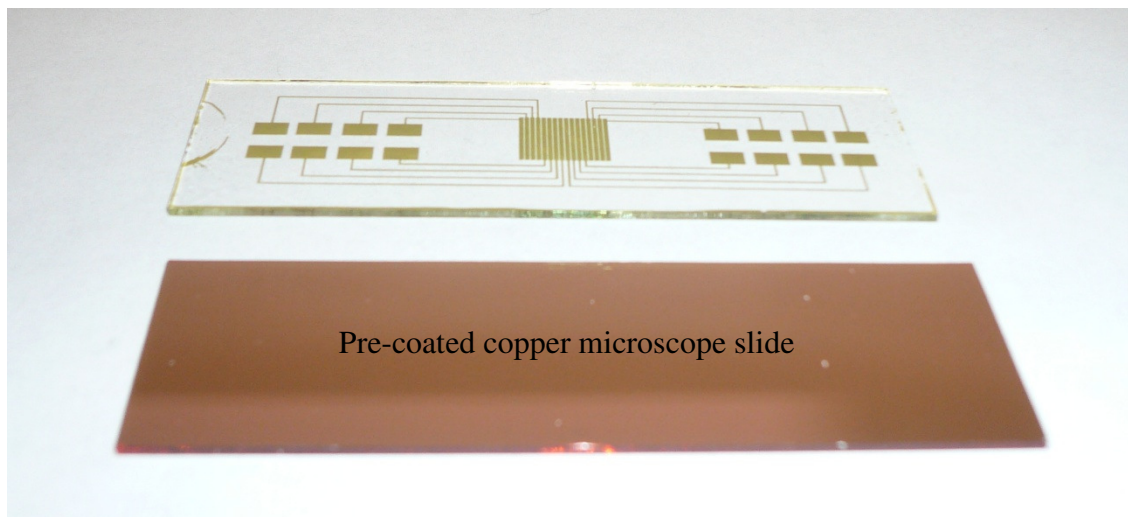
 Figure 4.7 A pre-coated copper microscope slide, and one of the fabricated DMF multiplexer prototypes are shown in this figure.
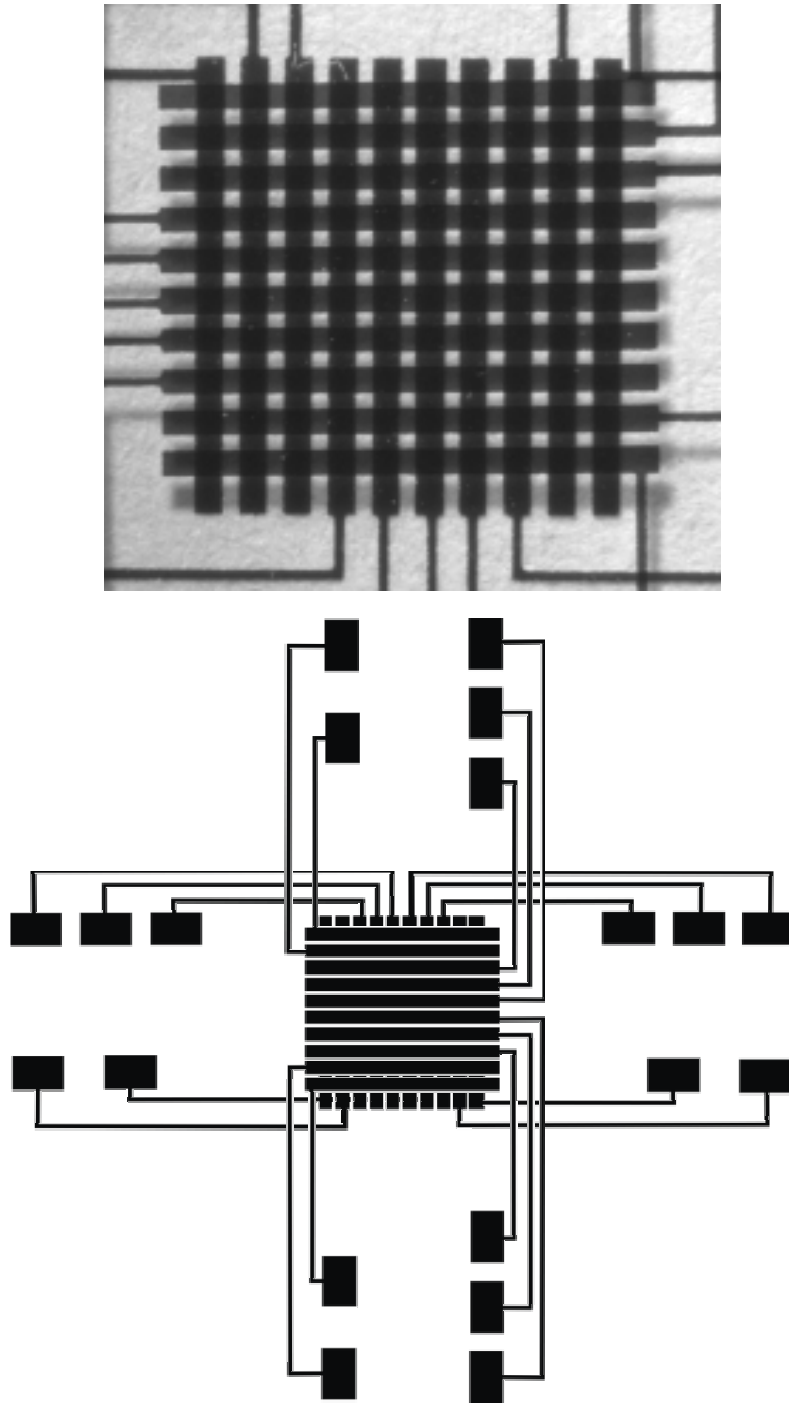
Figure 4.8 Final DMF multiplexer structure is shown in this figure. The fabricated DMF multiplexer prototype based on the presented recipe is shown at the top.

Chapter 5

5.1 Experimental Setup

Chapter 2 presented the results of the 2-D COMSOL simulation of a closed DMF system to illustrate the threshold voltage phenomenon. To verify these numerical results, several experiments have been conducted, and the threshold voltage phenomenon, as well as the DMF multiplexing format, has been studied experimentally.

5.2 Full Setup

The experimental setup used in this research is shown in Figure 5.1. As shown in this figure, a high-resolution camera, *xyz* translation stage and a 45° mirror are mounted on the optical table to acquire images of the microdroplet motion in the DMF multiplexer prototypes.

High-resolution camera   LED light   45° mirror

xyz stage

Figure 5.1 Final experimental setup.

5.3   High-Resolution Camera

Contact angle changes of microdroplets in a DMF system can be used to characterize numerous features of microdroplet motion. Analyzing the contact angle of the microdroplet at each instant shows the exact voltage at which the microdroplet starts to move. To do this analysis, the image of the microdroplet profile at each time is recorded with a high-resolution camera. Then, using the contact angle measurement program developed at the UBC DMF laboratory, the contact angle of the microdroplet at each time step is determined.

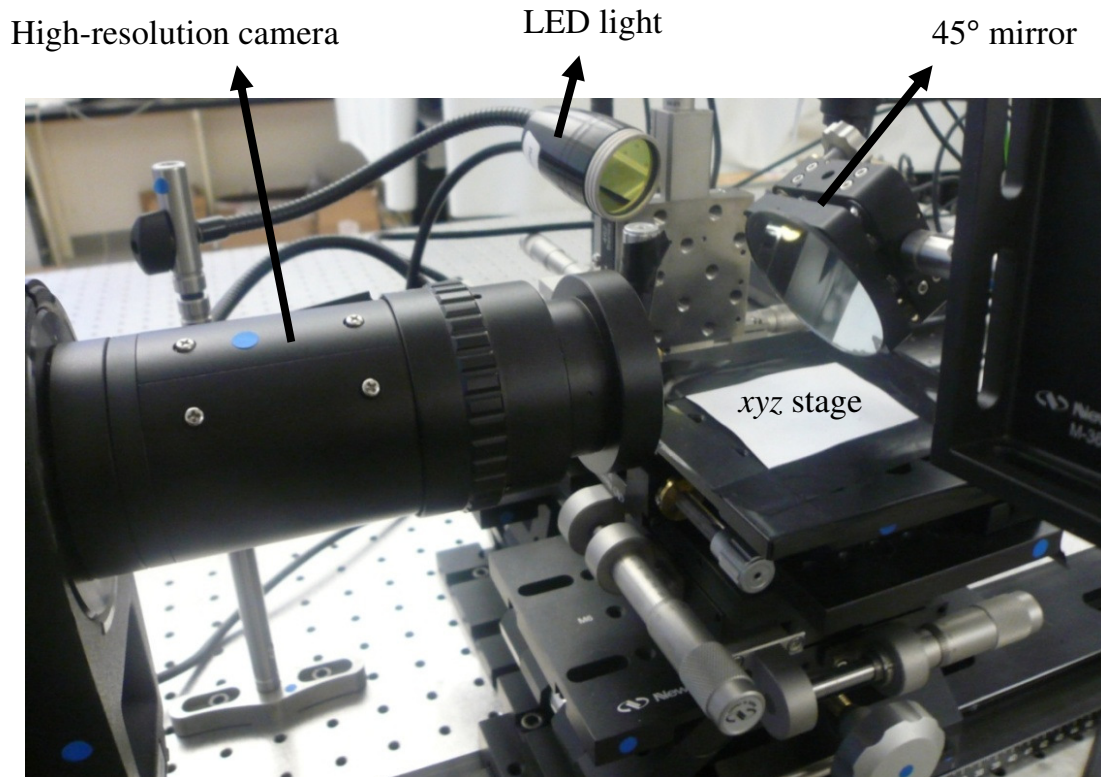An apochromatic microscope (LEICA APO Z6) connected to a high-resolution camera is used to record the motion of microdroplets within the DMF systems (see Figure 5.2). In this experimental setup, the high-resolution camera is mounted horizontally to acquire the profile images of the liquid microdroplet sandwiched between the top and bottom electrode plates of the closed DMF multiplexer.

The acquired images are then used to find the contact angle of the microdroplet at the three-phase contact line. An example of an acquired image from an open DMF system is shown in Figure 5.3. A contact angle measurement program based on automated polynomial fitting (APF) [32] is used to process the image. In this program, the Canny edge detection method finds the edge of the microdroplet, and a third-order polynomial is fitted to 120 points at the vicinity of the edge of the microdroplet. For this particular microdroplet, a contact angle of 115° is computed.
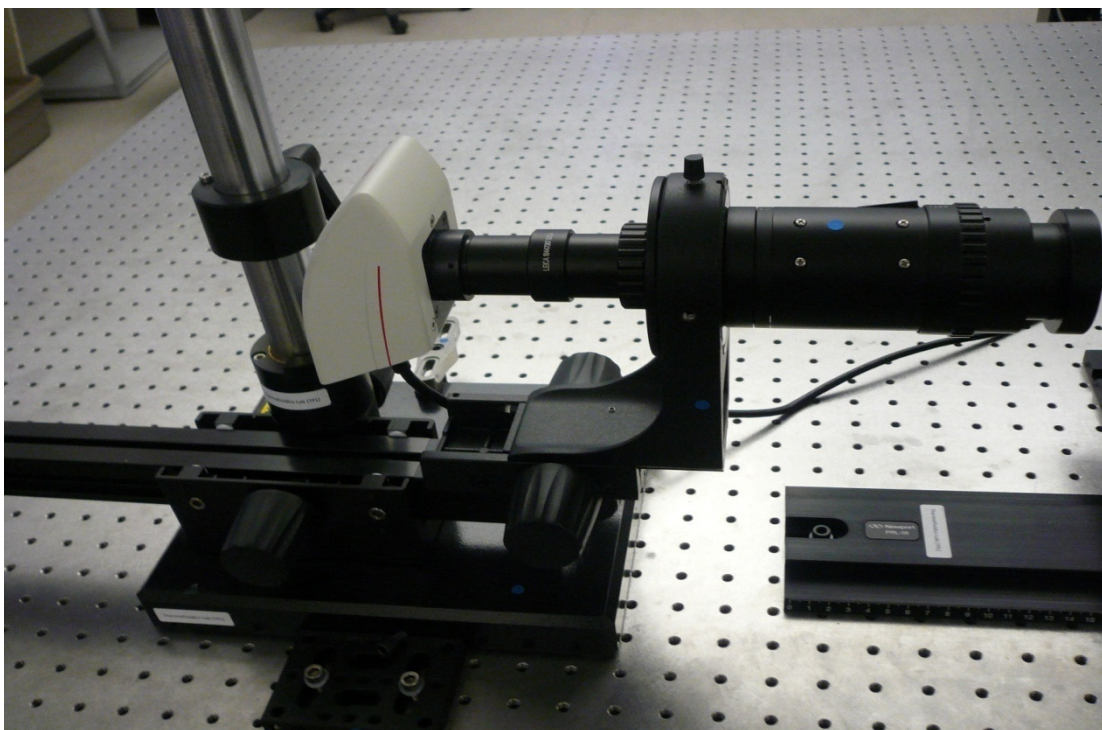
Figure 5.2 LEICA APO Z6, High-resolution camera/microscope setup.
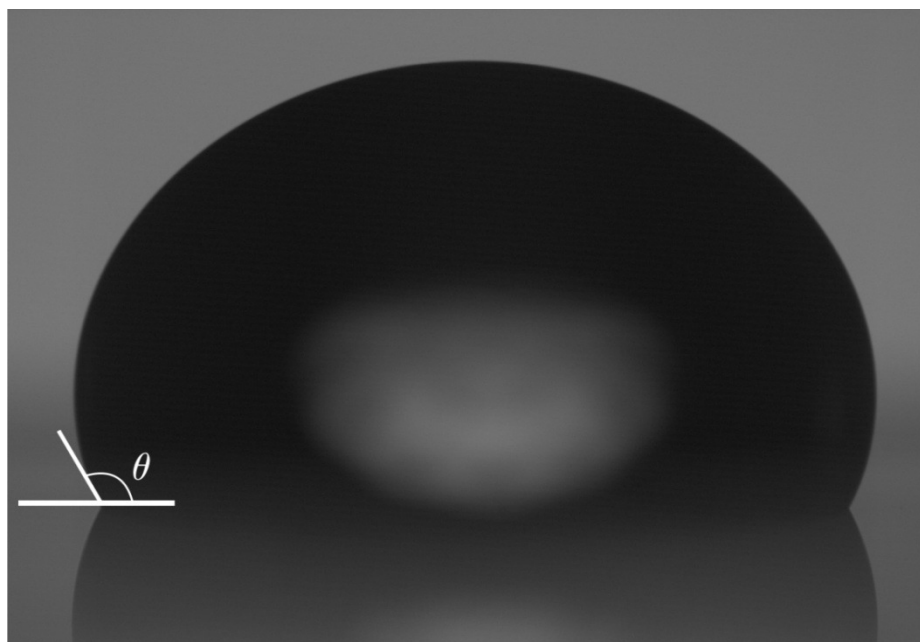
Figure 5.3 Image of a water microdroplet placed on the PDMS layer of an open DMF system acquired by the high-resolution camera.

5.4 Other Experimental Parts

Power Supply: One of the important parts of this experimental setup is the power supply. To control the applied voltage to the DMF system, a PS350/5000 V-25W high voltage power supply is used. This power supply has the ability to adjust the applied voltage and limit the electric current. Voltages between 0-5000 (V) can be applied.

Micropipettes: To have micro-litter liquid droplets, micropipettes must be used in the experimental setup. They can be adjusted for volumes between 0.1 µL to 20 µL. Typical microdroplet volumes used in this research are between 0.4-1.2 µL.

xyz Stage: In order to place the DMF prototypes in line with the high-resolution camera and have three degrees of freedom, an *xyz* translation stage is used. It is shown in Figure 5.4.

The high-resolution camera can be rotated about the *Y* axis, so the final setup will have four degrees of freedom. The DMF prototypes are clamped on this *xyz* translation stage. Then, the *X*, *Y* and *Z* lengths of the stage are adjusted in such a way that the microdroplet and prototype are in the middle of the high-resolution camera depth of focus.
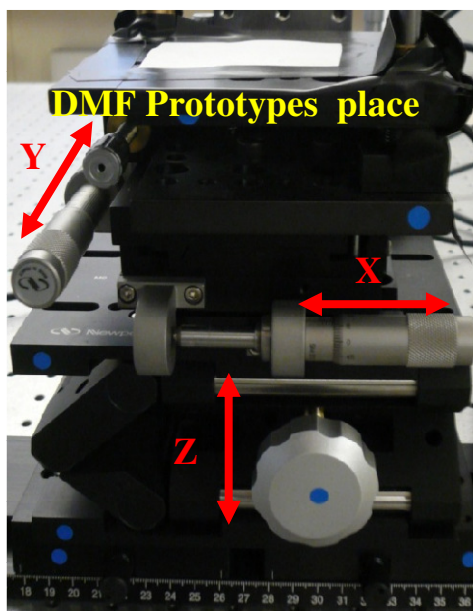
Figure 5.4 *xyz* translation stage.

5.5   Additional Experimental Challenges

Microdroplets can be seen from a top view in the experimental setup through the use of a mounted 45° mirror next to the *xyz* translation stage and high-resolution camera. There are still some challenges for the quality of these images, so methods to improve the visibility of the microdroplets in the acquired images are presented here:

1- Wider gaps between the adjacent electrodes in the designed DMF multiplexer masks yield better images. On the other hand, based on the previous chapter's conclusions, smaller gaps are needed in the proposed DMF multiplexer system to reduce the threshold voltage. Hence, there is a design tradeoff to satisfy both conditions.

2- Because of the very low current in the proposed DMF multiplexer device, thinner metal layers can be used to improve the image quality.

3- Indium tin oxide (ITO) can be used as the top plate to provide near-perfect transparency.

Chapter 6

6.1 Experimental Results

In this research, numerous experiments have been conducted to study experimentally the two aforementioned requirements of the proposed DMF multiplexer structure (namely the threshold voltage phenomenon and the multiplexing format based on the conventional cross-referencing architecture). The results of these experiments are presented in the following two subsections.

6.1.1 Experimental Verification of the Significance of Threshold Voltage

In order to study the significance of the threshold voltage phenomenon, a closed DMF system is designed and fabricated. The reported fabrication recipe in Chapter 4 is used. For the grounded top plate, a copper microscope slide is covered with a PDMS layer and then cured in the oven for 24 hours at 150℃ . Also, two 250 µm spacers are placed between the top and bottom plates to create a constant gap height. The water microdroplet is sandwiched between the top and bottom plates. The schematic of this closed DMF system is shown in Figure 6.1.
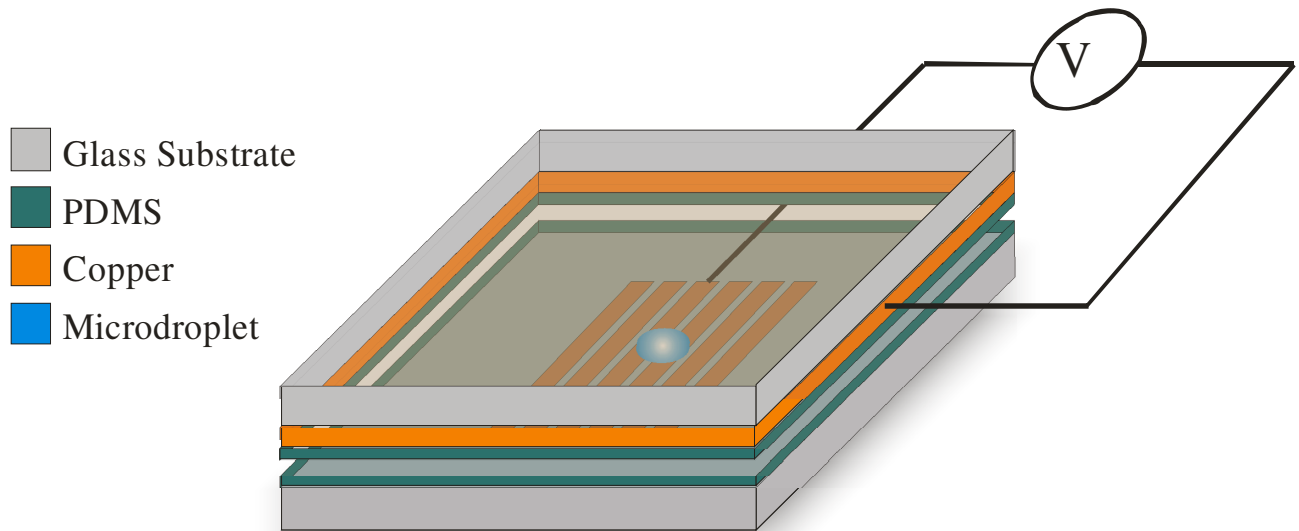

Figure 6.1 3-D schematic of a closed DMF system.

Before applying voltages to the electrode under the microdroplet, all the surfaces in contact with the microdroplet are hydrophobic, and the water microdroplet is completely symmetric (i.e.

all the contact angles are the same (114°)). After applying a voltage, there exists a possibility for microdroplet asymmetry and deflection.

As shown in Figure 6.2, at voltages below the threshold voltage (on the right bottom electrode), the contact angle change of the microdroplet edge over the activated electrode is very small. In this case, the EWOD forces are smaller than the static friction forces between the microdroplet and the PDMS layer, so the microdroplet cannot move towards the activated electrode.

Figure 6.2 A cross-sectional image of a closed DMF system acquired by the high-resolution camera at a voltage below the threshold voltage is shown in this figure.

By increasing the applied voltage, the contact angle of the microdroplet can be made to decrease as the PDMS surface becomes hydrophilic. However, this does not occur until the applied voltage reaches the threshold voltage V_{th}. Figure 6.3 shows this point. At the threshold voltage, the EWOD forces are large enough to overcome the friction forces between the

microdroplet and the PDMS layer, and the microdroplet starts to move. Also, the contact angle change of the microdroplet becomes noticeable.
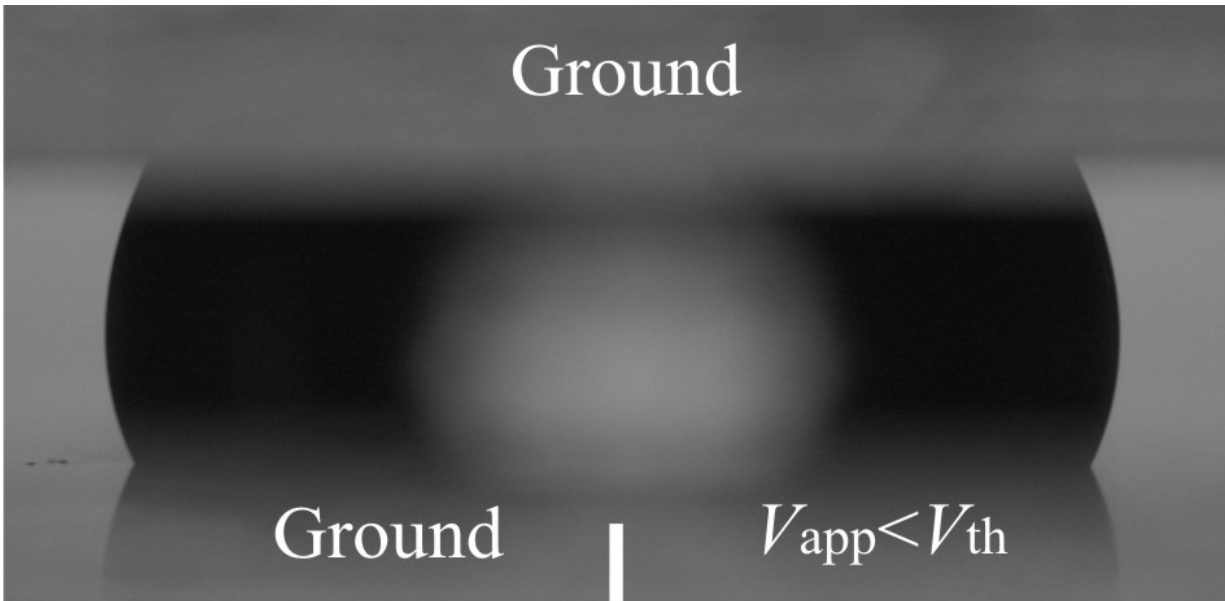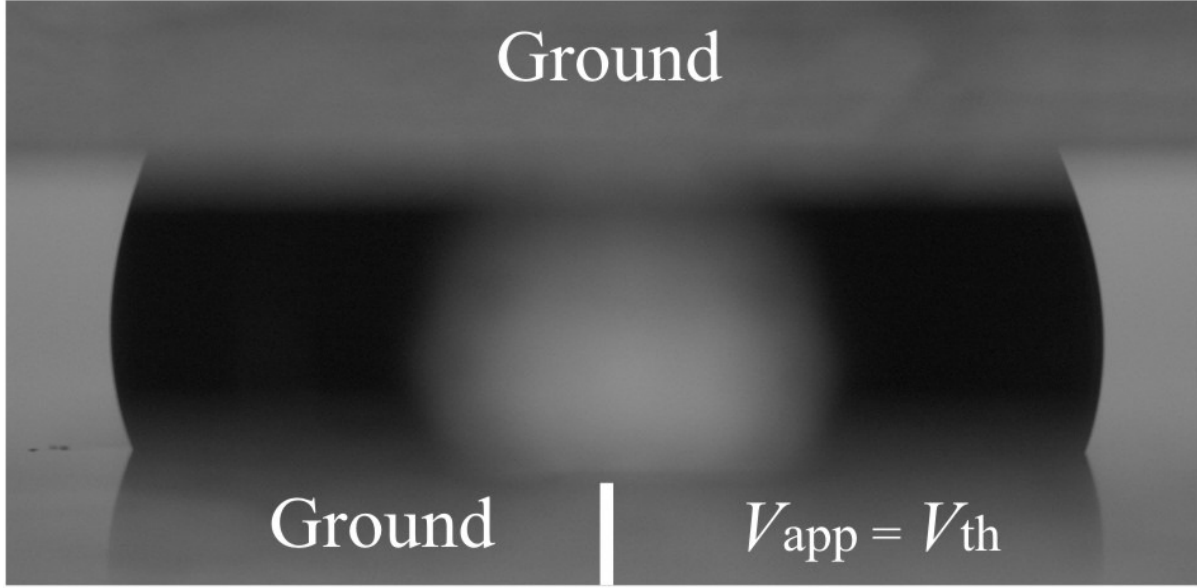

Figure 6.3 Cross-sectional image of a closed DMF system acquired by the high-resolution camera at the threshold voltage is shown in this figure. The contact angle change of the right bottom edge of the microdroplet is visible, and the microdroplet has started to move.

At voltages beyond the threshold voltage, the microdroplet moves faster, and the contact angle change is greater than the contact angle change at the threshold voltage. The change of contact angle for voltages after the threshold voltage is shown in Figure 6.4.

The complete characterization for the contact angle versus V_{app} relationship is presented in Figure 6.5. The presence of a threshold condition in the experimental data at $V_{th} = 160$ V is readily apparent. This meets the first requirement for 2-D localization in the proposed DMF multiplexer. For voltages in the range 160 V to 220 V, the contact angle changes correspond to those predicted by the Lippmann-Young equation (Eq.(11)) [33, 34]. At voltages beyond 220 V, saturation effects begin to affect the contact angles, and the validity of the Lippmann-Young equation is reduced. The threshold voltage of $V_{th} = 160$ V seen here is a characteristic of the device geometry tested here (incorporating PDMS and a vertical plate separation of

250 μm). The threshold voltage can be reduced, as needed, by application-specific selection of dielectric and hydrophobic layer materials (Teflon AF and Parylene C) and reduced thicknesses.
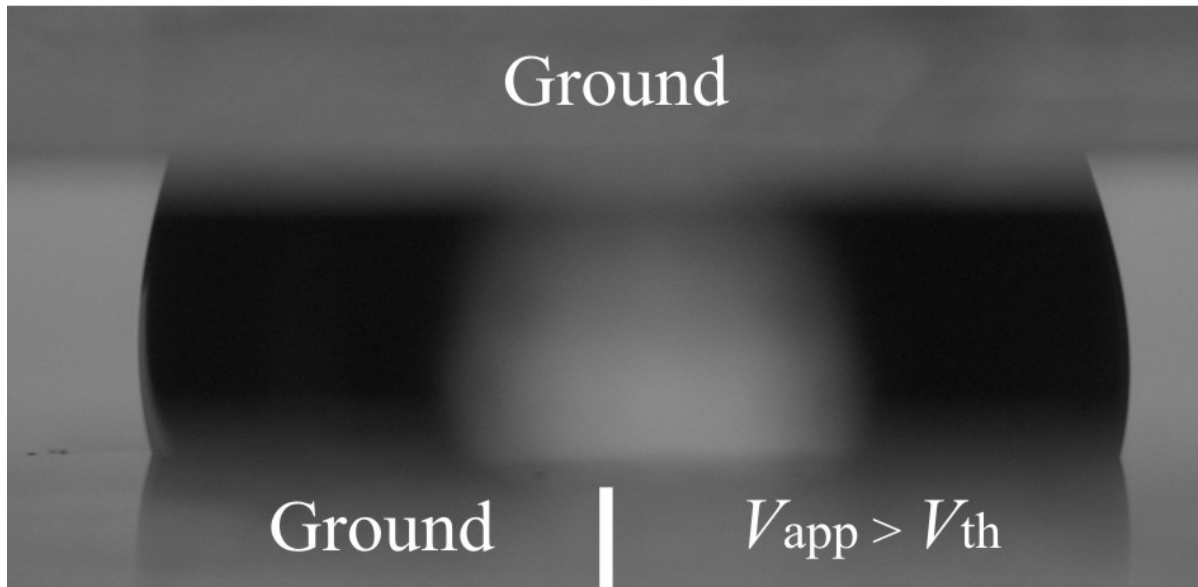

Figure 6.4 Contact angle change of the right bottom edge of the microdroplet at a voltage greater than the threshold voltage is shown in this figure.
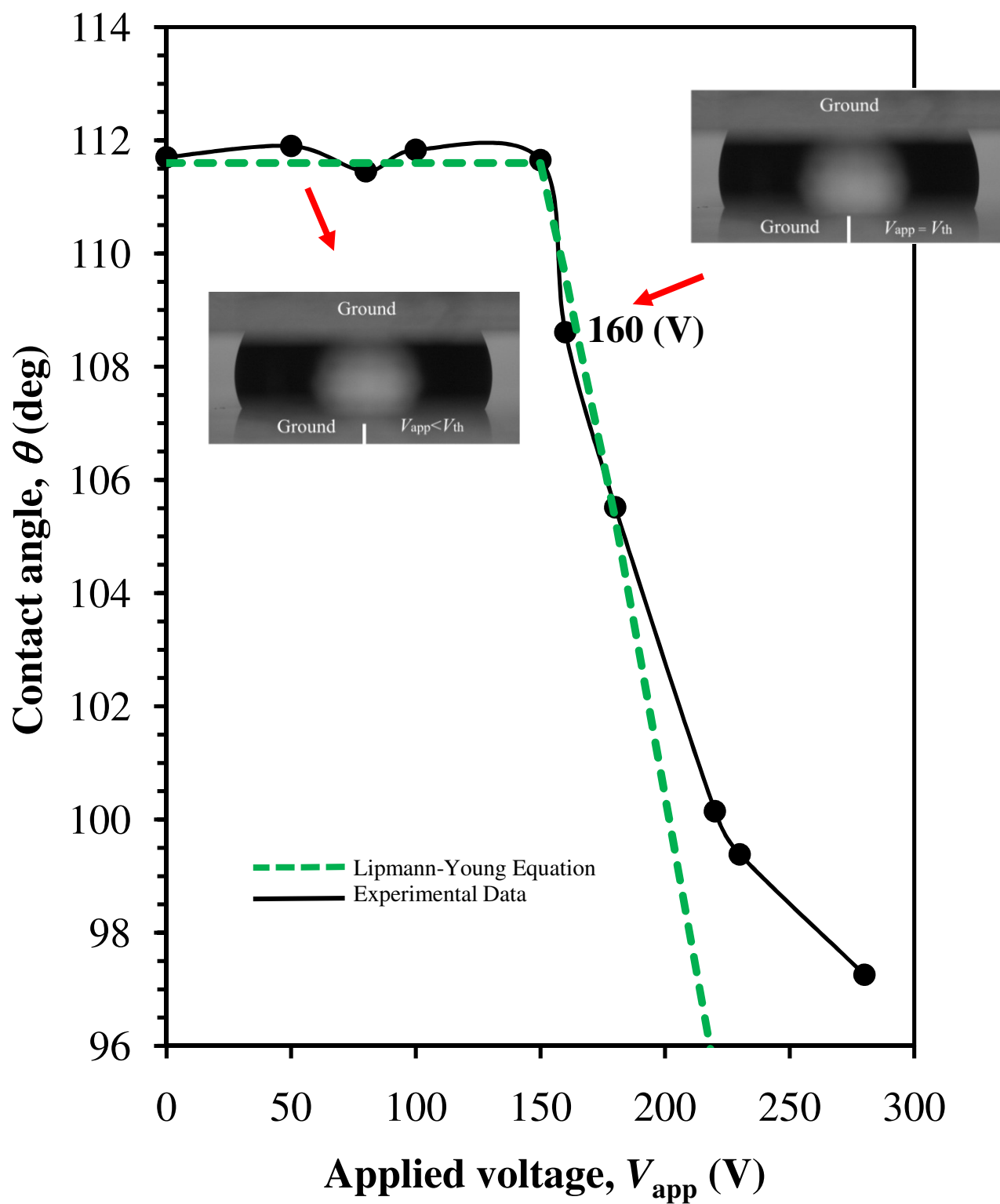
Figure 6.5 Experimental results of the contact angle change versus the applied voltage are shown for the closed DMF system.

The COMSOL simulation results of Chapter 2, regarding the threshold voltage phenomenon in a closed DMF system, can be verified by the above experimental results. The numerical results produced by the modified level-set method with the corresponding microdroplet profiles exhibited a clear threshold condition. When the applied voltage is at or below the threshold voltage, very little contact angle change is witnessed. However, when the applied voltage is above the threshold voltage, a contact angle change is apparent. This threshold condition is also witnessed through experimental observation with a closed DMF structure. These experimental results are shown in Figures 6.6 (d-f). At a voltage of 150 V, very little contact angle changes are observed, and this immobility remains until the applied voltage reaches the $V_{th} = 160$ V (i.e. the threshold condition). Above this voltage the contact angle is greatly reduced.
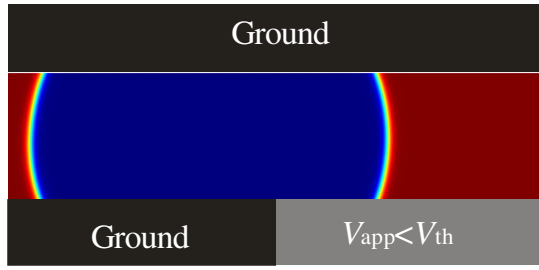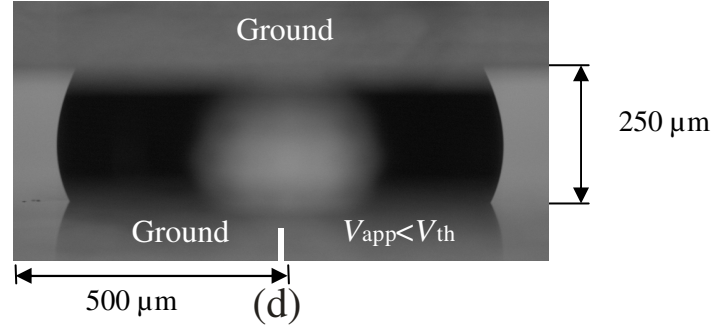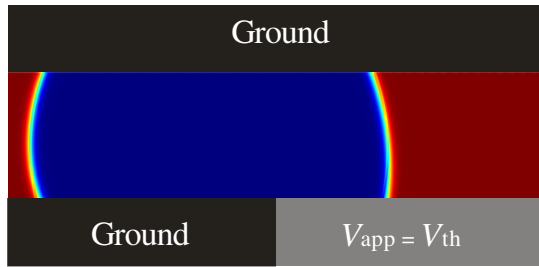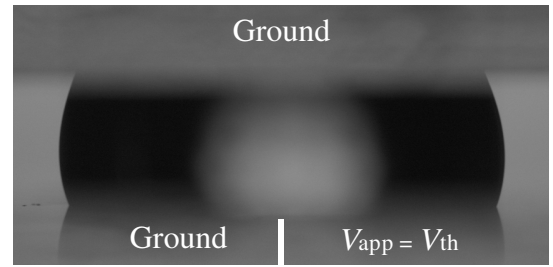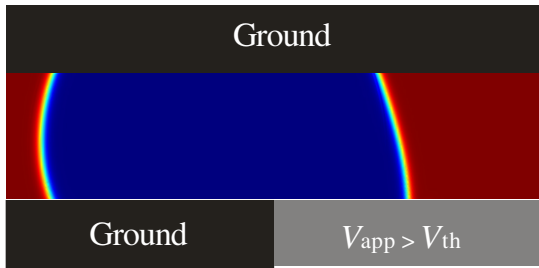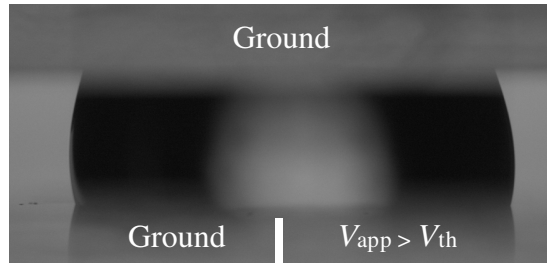
Figure 6.6 Results are shown for a microdroplet in a closed DMF system with a threshold voltage of $V_{th} = 160$ V. Numerical results are shown for an applied voltage (a) below the threshold voltage, (b) at the threshold voltage and (c) above the threshold voltage. Experimental images are shown for the same system with the applied voltage (d) below the threshold voltage, (e) at the threshold voltage and (f) above the threshold voltage. The copper electrodes are coated with PDMS and separated by a distance of 250 μm.

6.1.2 Experimental Validation of the Multiplexer Protocol

Two requirements of the proposed DMF multiplexer system have been studied numerically in the previous chapters. In this section, the proposed multiplexing format of the DMF multiplexer prototype is studied experimentally. Motion of the desired microdroplet in a cross-referencing architecture through bi-polar voltage activation and threshold-based voltage actuation is shown.

Different DMF multiplexer systems have been designed and fabricated using the reported fabrication recipe of Chapter 4. Wires are soldered onto the connecting pads from one side and passed into a multi channel switch box.

The *X* electrode array of the DMF multiplexer systems is mounted on an *xyz* translation stage, and two microdroplets with the same volume, 0.6 µL, are deposited on the PDMS layer. Then, the *Y* electrode array is placed orthogonally to the bottom plate with two 250 µm spacers acting as separators between the top and bottom electrode plates.

Figure 6.7 shows the first experimental results of the proposed multiplexing protocol. Images of microdroplets within the DMF multiplexer during bi-polar voltage activation are shown in this figure. The onset of the motion, being of relevance to the threshold-based voltage actuation, is recorded by the high-resolution camera. Because of the large gap between adjacent electrodes, pairs of electrodes are used to provide the bi-polar activation in this case. The onset of motion is readily apparent in this figure for the lower microdroplet, which is located in the high-field region of the structure. Note that the top microdroplet, which does not experience a doubling of the voltage difference due to bi-polar activation, does not begin moving. Indeed, the threshold-based voltage actuation and bi-polar cross-referenced structure can, together, allow for complete 2-D addressability in this case. Subsequent bi-polar signals can be used to actuate the microdroplet in this 2-D plane.

(a)

(b)
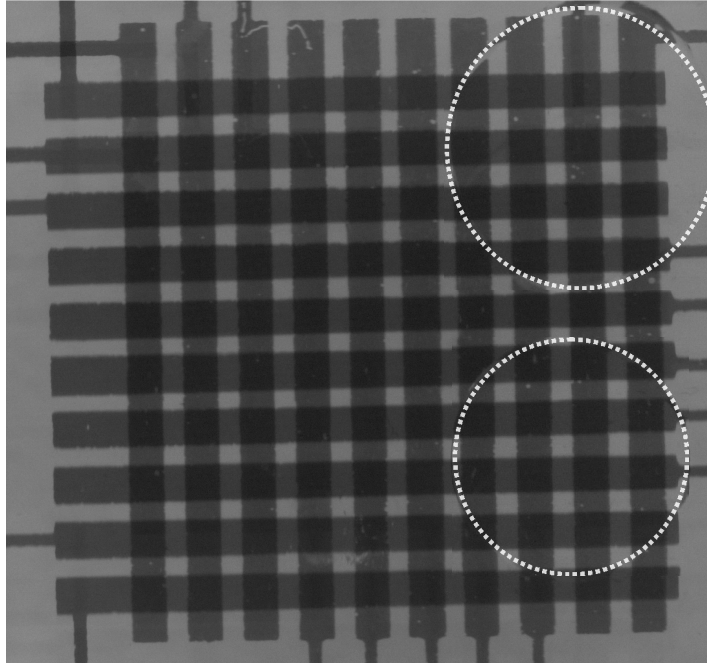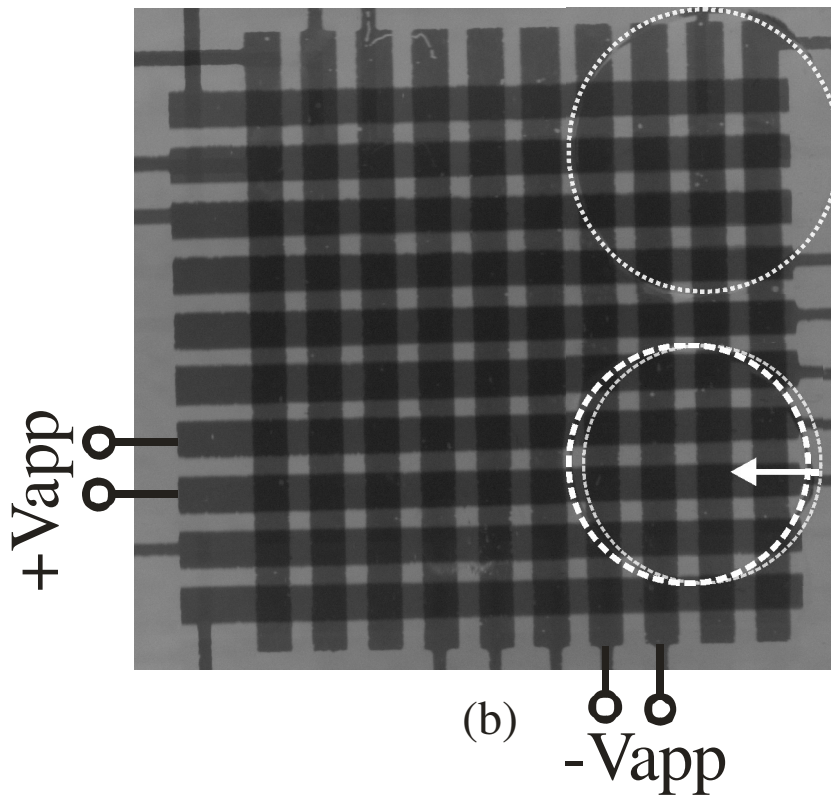
+Vapp

-Vapp

Figure 6.7 Experimental results are shown for the fabricated chip with (a) no voltage applied and (b) -V_{app} applied to two bottom electrodes and +V_{app} applied to two top electrodes.

Figure 6.8 shows two similar microdroplets placed on the same electrode row. The right microdroplet moves, and the left is stationary.

The complete motion of a microdroplet is shown in Figure 6.9 for the case with $+V_{app}$ applied to the third bottom electrode and $-V_{app}$ applied to the second top electrode. In this case, due to the smaller gap sizes between the adjacent electrodes (150 µm), only one of the electrodes has been activated.
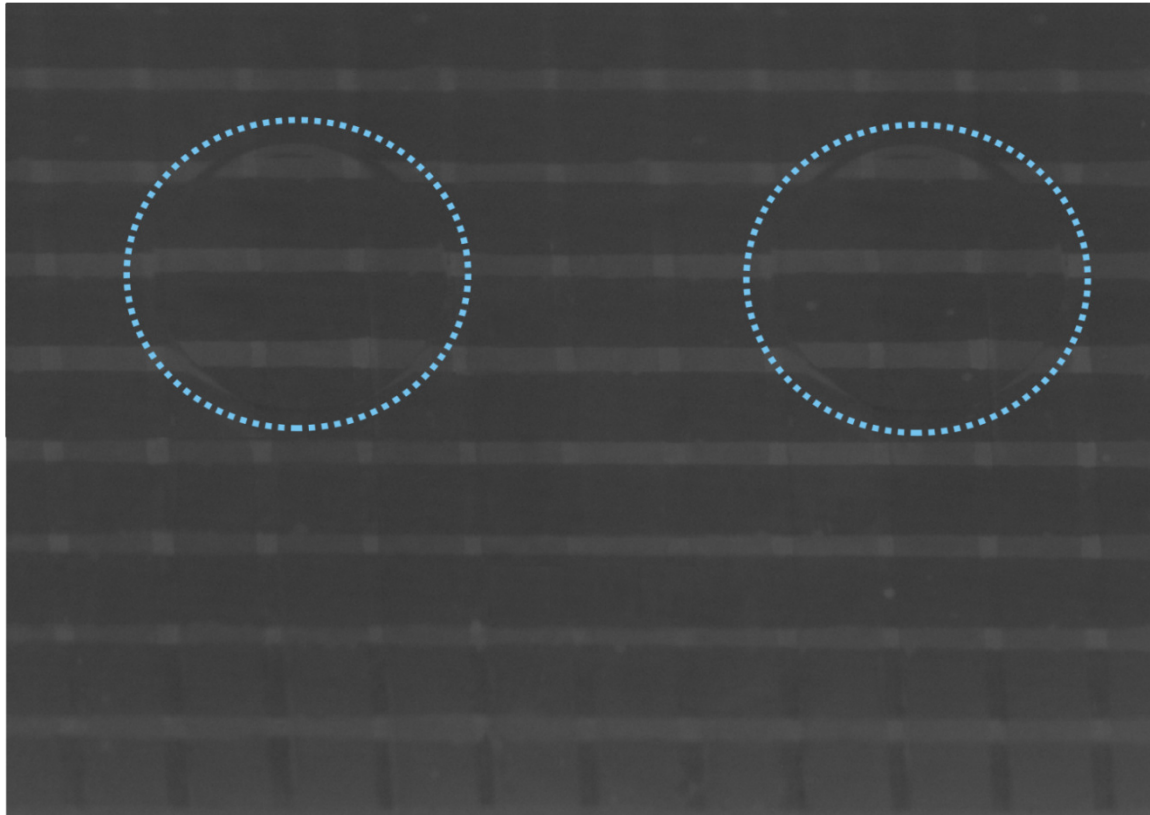
Figure 6.8 Two 0.6 µL microdroplets are sandwiched between the top and bottom electrode arrays in the fabricated DMF multiplexer system. Each electrode width is 500 µm and the gap size between the adjacent electrodes is 150 µm.

The next presented experimental results of the fabricated DMF multiplexer prototypes are shown in Figures 6.10 (a, b). Figure 6.10 (a) shows two microdroplets placed on different electrode rows. The left microdroplet moves, while the right one is stationary. The desired motion in this experiment is diagonal motion to the cell placed on the right bottom of the current

position of the microdroplet. To do this, $+V_{app}$ is applied to the fourth bottom electrode column, and $-V_{app}$ is applied to the second top electrode row.

Figure 6.10 (b) shows that the left microdroplet, experiencing $2V_{app}$ electric potential, has moved to its desired position, while the right microdroplet is still at its initial position.

Figure 6.9 Experimental results are shown for the fabricated chip. By applying $+V_{app}$ and $-V_{app}$ to the third bottom and second top electrodes respectively, the right microdroplet experiencing $2V_{app}$ electric potential, moved completely to the next top electrode row while at the same time, the stationary microdroplet, experiencing $|-V_{app}| < |V_{th}|$ did not move.
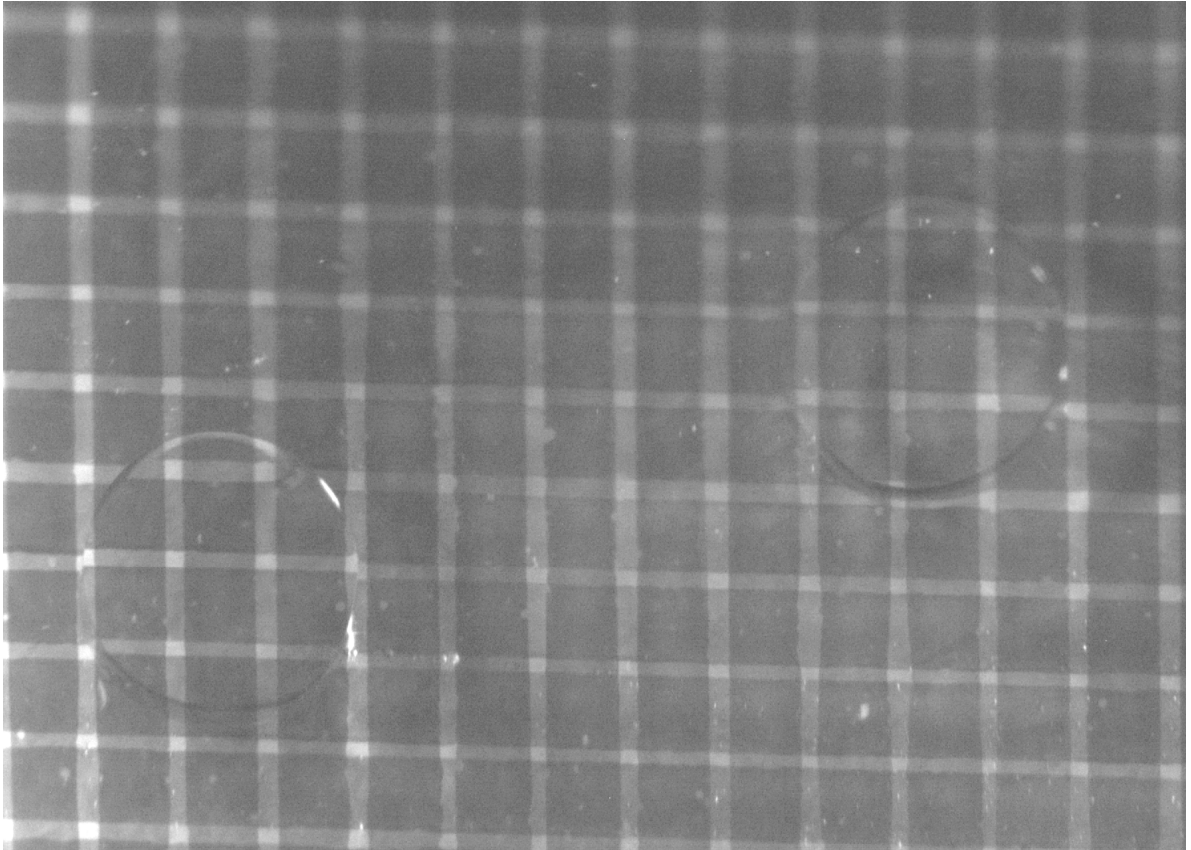
(a)
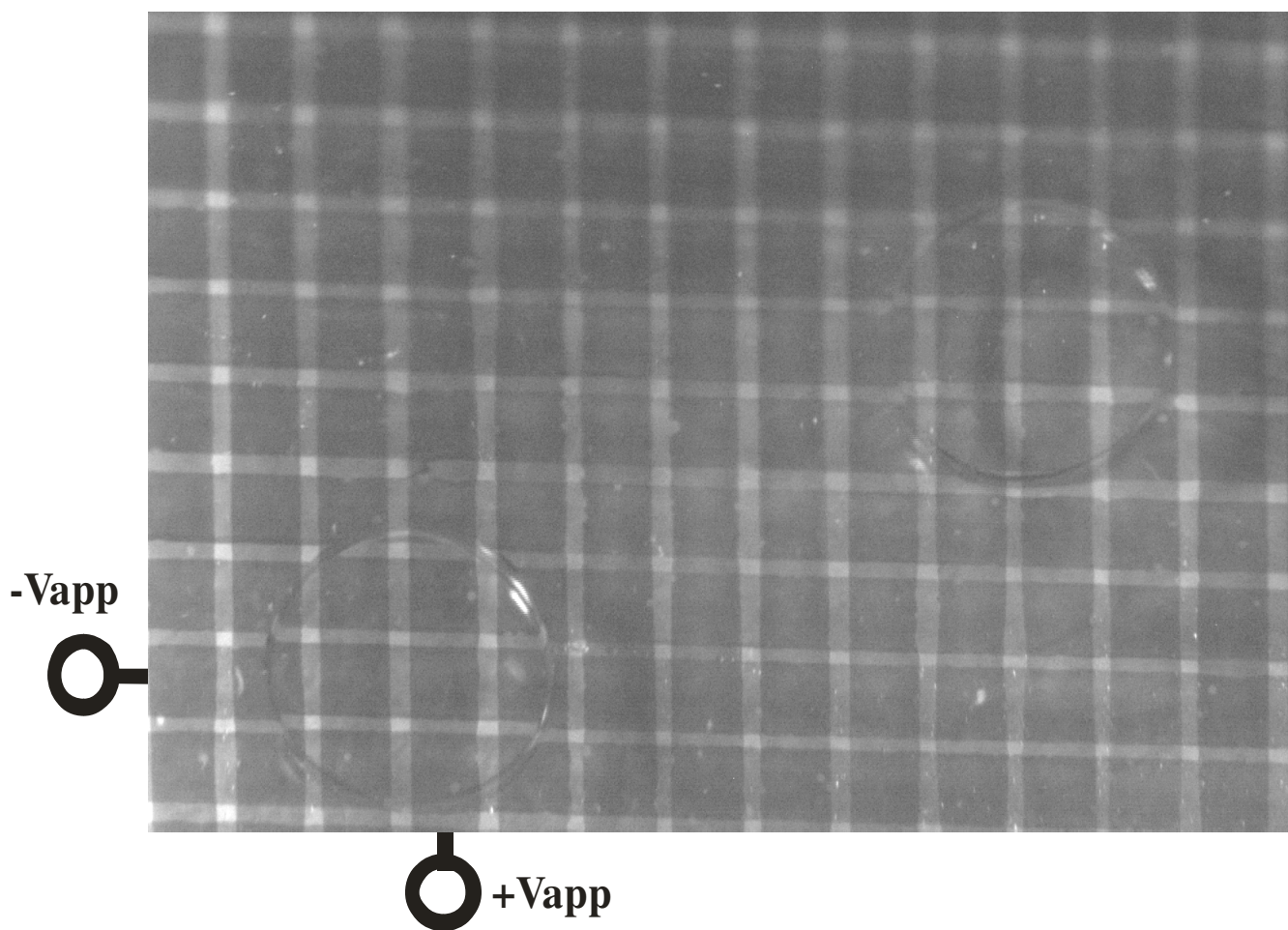
(b)

Figure 6.10 Diagonal motion of a microdroplet in a DMF multiplexer system is shown in this figure. (a) Two equal 0.5 µL microdroplets are sandwiched between the top and bottom electrode plates. (b) The left microdroplet is moved to the right bottom cell position due to experiencing $2V_{app}$ electric potential at this position while the right microdroplet is stationary.

To improve the quality of the acquired images with the high-resolution camera, an LED light is projected onto the cross-section of the mounted DMF multiplexer on the *xyz* translation stage. The new results, with the improved imaging quality, are presented in Figures 6.11 and 6.12.
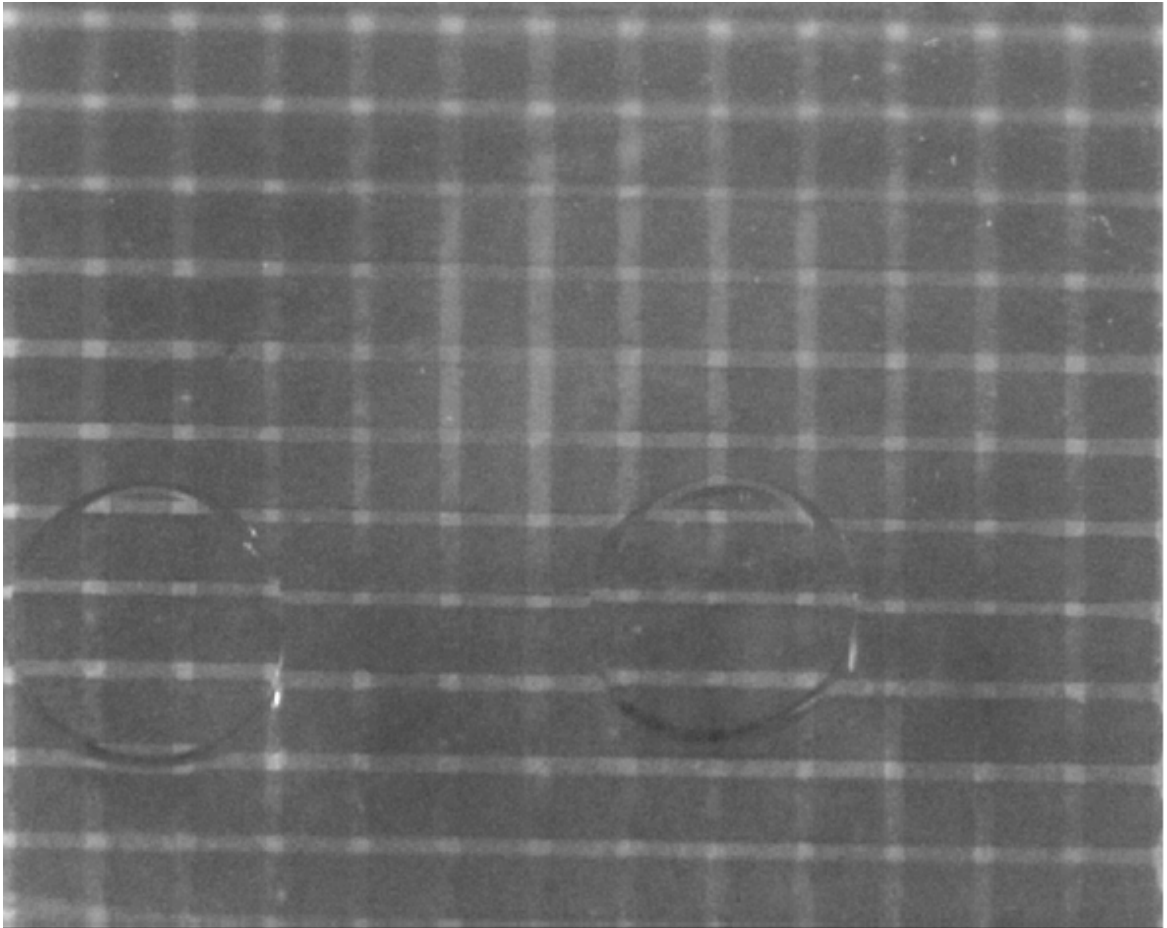
Figure 6.11 Two microdroplets are placed on the same electrode row in the fabricated DMF multiplexer system. The left microdroplet is the moving one and right one is stationary.

As shown in Figure 6.11, adding the LED light has increased the image quality. In this figure, two microdroplets are completely visible.
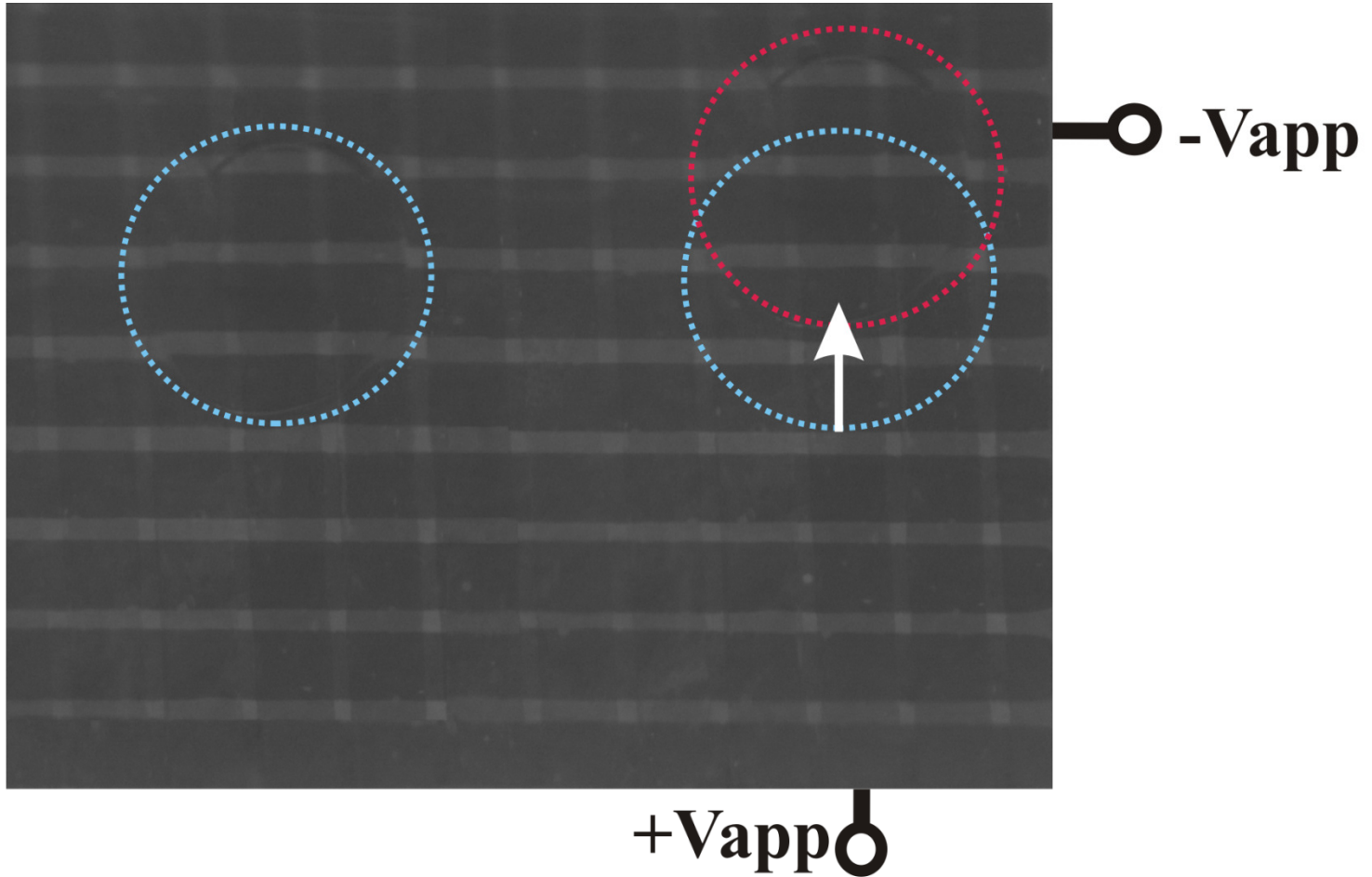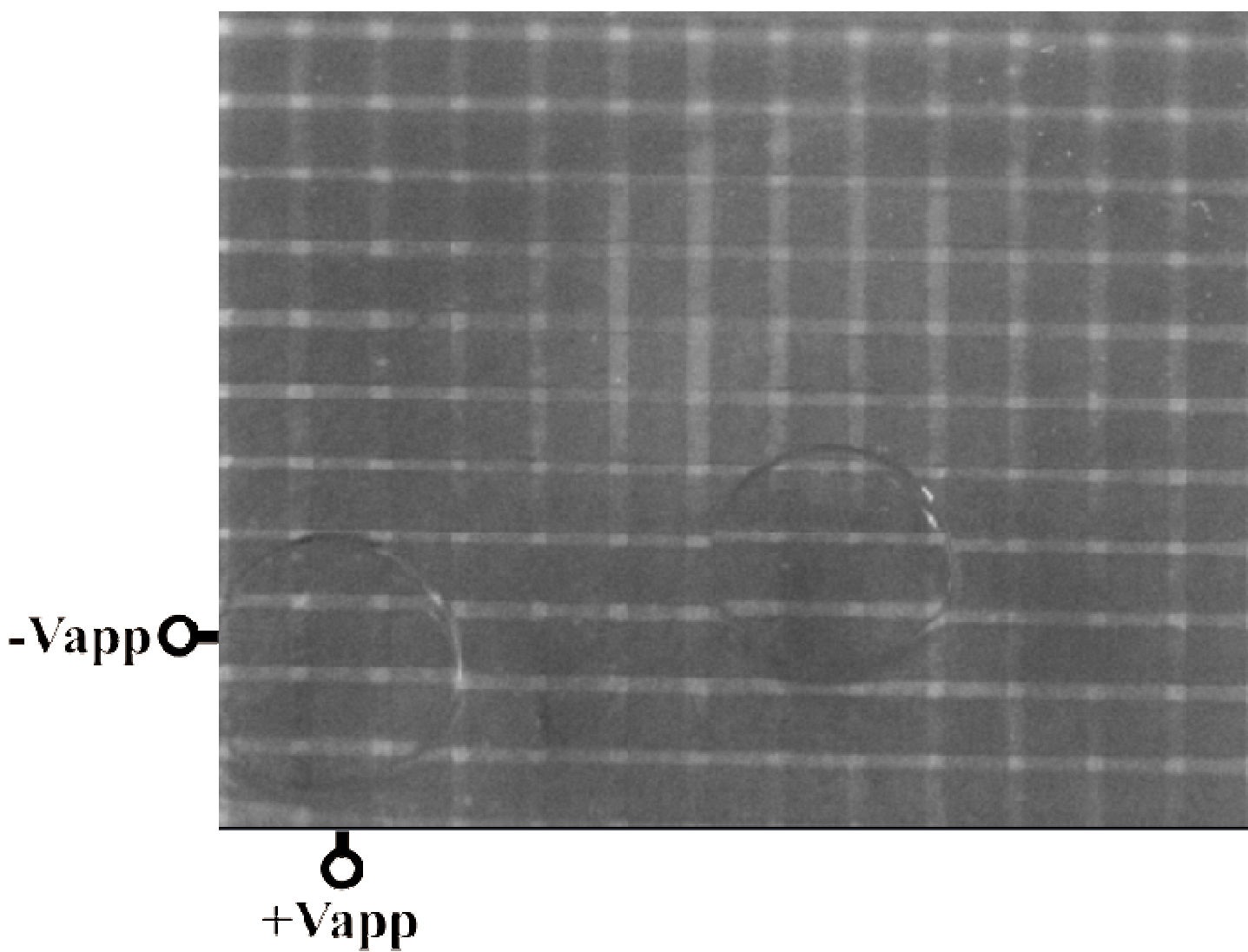
Figure 6.12 Experimental results are shown for the fabricated chip. By applying +Vapp and -Vapp to the second bottom and third top electrodes, the left microdroplet, experiencing 2Vapp electric potential, moves vertically to the bottom cell, while at the same time, the stationary microdroplet, experiencing |-V_{app}| < |V_{th}| did not move.

Chapter 7

7.1 Conclusions

In this research independent motion of microdroplets in a cross-referenced DMF structure was achieved for systems incorporating multiple microdroplets. To accomplish this motion, a multiplexing format was implemented into the conventional cross-referenced architecture to satisfy threshold-based voltage actuation and bi-polar voltage activation. These two requirements were studied numerically and the results verified experimentally.

Modelling and simulation of microdroplet motion in a closed DMF structure was achieved with COMSOL. The threshold voltage phenomenon was introduced in chapter 2. Each DMF system has a threshold voltage below which the microdroplet would not start to move. At the threshold voltage, the microdroplet moves to the neighboring electrode, and beyond this magnitude the microdroplet moves faster.

3-D simulation of the proposed DMF multiplexer system in COMSOL showed the enhanced localization of the electric field at the intersection of the activated electrodes (+V_{app} on the top electrode and -V_{app} on the bottom electrode). The electric field created by the overlapped electrodes was greater than that in all other regions.

Regarding the experimental results, a fabrication recipe was reported to fabricate the closed DMF structures for threshold voltage validation and the bi-polar voltage activation scheme. Pre-coated copper microscope slides were used as the top and bottom electrode arrays. Masks were designed in CorelDRAW and printed on a transparency film. PDMS was used as both the hydrophobic and dielectric layers. A high-resolution camera was used to acquire the microdroplet motion between the fabricated DMF multiplexer electrode arrays.

Although the proposed multiplexing format increases the flexibility of the digital microfluidic systems in simultaneous manipulation of multiple microdroplets, there are still some limitations for more complicated assays involving a greater number of microdroplets. For example, if there are three microdroplets aligned along a single column electrode and the intention is to move the top microdroplet to the left cell and the bottom one to the right cell, the middle microdroplet cannot move upward or downward simultaneously. However, the scheduling problem can be

simplified using the proposed format. In this example, the middle microdroplet should wait one time step for the top and bottom microdroplets to move to their desired destination cells whereas in a traditional cross-referencing the same microdroplet must wait two steps.

The proposed multiplexer structure will have a significant impact on the application of digital microfluidic systems in the biomedical applications especially where simultaneous motions of multiple microdroplets are desired for high throughput screening (HTS) assays. For example, a glucose assay biochip can be designed and fabricated to work with the proposed DMF multiplexer system and measure the glucose amount of a blood sample. Indeed with the proposed multiplexing protocol more flexibility and scalability will be achieved in the system due to the parallelization of this format compared to the conventional closed DMF systems.

The device met the two requirements for enhanced $m \times n$ addressability in a 2-D grid, and results were shown both experimentally and numerically. Successful actuation without disturbing neighboring microdroplets was demonstrated through this threshold-voltage-based technique. The technique was presented with positive and negative voltages on the row and column electrodes; although, interestingly, the same principle can be applied with AC voltage sources and a 1:1 transformer providing $V_{app} \angle 0°$ and $V_{app} \angle 180°$ on the row and column electrodes.

7.2 Future Work

Extension of this research will relate to sequential motion of microdroplets in the DMF multiplexer. Mixing, merging and splitting of two microdroplets also will be done. Moreover, decreasing the threshold voltage in the multiplexer prototypes is considered to be one of the important future goals of this novel research. Certain applications (e.g., those containing bio-species) have limitations on the voltages that can be applied; thus a reduction in the threshold voltage will open the door to a wider variety of microfluidic applications.

Bibliography

[1] S. K. Fan, P. P. Guzman and C. J. Kim, "EWOD driving of droplet on NxM grid using single layer electrode patterns," in *Solid-State Sensor, Actuator, Microsystems Workshop,* 2002, pp. 134–137.

[2] S. K. Fan, C. Hashi and C. J. Kim, "Manipulation of multiple droplets on NxM grid by cross-reference EWOD driving scheme and pressure-contact packaging," in *IEEE MEMS,* 2003, pp. 694-697.

[3] T. Xu and K. Chakrabarty, "A cross-referencing-based droplet manipulation method for high-throughput and pin-constrained digital microfluidic arrays," in *Proceedings of the Conference on Design, Automation and Test in Europe,* 2007, pp. 552-557.

[4] R. B. Fair, A. Khlystov, T. D. Tailor, V. Ivanov, R. D. Evans, V. Srinivasan, V. K. Pamula, M. G. Pollack, P. B. Griffin and J. Zhou, "Chemical and biological applications of digital-microfluidic devices," *IEEE Des. Test Comput.,* vol. 24, pp. 10-25, 2007.

[5] V. Srinivasan, V. K. Pamula, P. Paik and R. B. Fair, "Protein stamping for MALDI mass spectrometry using an electrowetting- based microfluidic platform," in *SPIE Conference,* 2004, pp. 26-32.

[6] A. R. Wheeler, H. Moon, C. A. Bird, R. R. O. Loo, C. Kim, J. A. Loo and R. L. Garrell, "Digital microfluidics with in-line sample purification for proteomics analyses with MALDI-MS," *Anal. Chem.,* vol. 77, pp. 534–540, 2005.

[7] V. Srinivasan, V. K. Pamula and R. B. Fair, "An integrated digital microfluidic lab-on-a-chip for clinical diagnostics on human physiological fluids," *Lab on a Chip,* vol. 4, pp. 310-315, 2004.

[8] V. Srinivasan, V. K. Pamula and R. B. Fair, "Droplet-based microfluidic lab-on-a-chip for glucose detection," *Anal. Chim. Acta,* vol. 507, pp. 145-150, 2004.

[9] M. J. Madou, *Fundamentals of Microfabrication: The Science of Miniaturization.* CRC, 2002.

[10] G. T. A. Kovacs, *Micromachined Transducers Sourcebook.* Boston, 1998.

[11] C. M. Ho, "Fluidics-the link between micro and nano sciences and technologies," in *Micro Electro Mechanical Systems, 2001. MEMS 2001. the 14th IEEE International Conference on,* 2001, pp. 375-384.

[12] M. G. Pollack, R. B. Fair and A. D. Shenderov, "Electrowetting-based actuation of liquid droplets for microfluidic applications," *Appl. Phys. Lett.,* vol. 77, pp. 1725, 2000.

[13] J. Ding, K. Chakrabarty and R. B. Fair, "Scheduling of microfluidic operations for reconfigurable two-dimensional electrowetting arrays," *IEEE Transactions on Computer Aided Design of Integrated Circuits and Systems,* vol. 20, pp. 1463-1468, 2001.

[14] S. K. Cho, H. Moon and C. J. Kim, "Creating, transporting, cutting, and merging liquid droplets by electrowetting-based actuation for digital microfluidic circuits," *Microelectromechanical Systems,* vol. 12, pp. 70-80, 2003.

[15] Y. H. Chang, G. B. Lee, F. C. Huang, Y. Y. Chen and J. L. Lin, "Integrated polymerase chain reaction chips utilizing digital microfluidics," *Biomed. Microdevices,* vol. 8, pp. 215-225, 2006.

[16] I. Barbulovic-Nad, H. Yang, P. S. Park and A. R. Wheeler, "Digital microfluidics for cell-based assays," *Lab on a Chip,* vol. 8, pp. 519-526, 2008.

[17] E. A. Ottesen, J. W. Hong, S. R. Quake and J. R. Leadbetter, "Microfluidic digital PCR enables multigene analysis of individual environmental bacteria," *Science,* vol. 314, pp. 1464, 2006.

[18] J. Lee, H. Moon, J. Fowler, T. Schoellhammer and C. J. Kim, "Electrowetting and electrowetting-on-dielectric for microscale liquid handling," *Sensors & Actuators: A.Physical,* vol. 95, pp. 259-268, 2002.

[19] H. Moon, S. K. Cho and R. L. Garrell, "Low voltage electrowetting-on-dielectric," *J. Appl. Phys.,* vol. 92, pp. 4080, 2002.

[20] C. Quilliet and B. Berge, "Electrowetting: a recent outbreak," *Current Opinion in Colloid & Interface Science,* vol. 6, pp. 34-39, 2001.

[21] J. Berthier, *Microdrops and Digital Microfluidics: Processing, Development, and Applications.* William Andrew Publishing, 2007.

[22] M. G. Pollack, A. Shenderov and R. B. Fair, "Electrowetting-based actuation of droplets for integrated microfluidics," *Lab on a Chip,* vol. 2, pp. 96-101, 2002.

[23] M. Sussman, P. Smereka and S. Osher, "A level set approach for computing solutions to incompressible two-phase flow," *Journal of Computational Physics,* vol. 114, pp. 146-159, 1994.

[24] J. Sethian and P. Smereka, "Level set methods for fluid interfaces," *Annu. Rev. Fluid Mech,* vol. 35, pp. 341-372, 2003.

[25] D. Peng, B. Merriman, S. Osher, H. Zhao and M. Kang, "A PDE-based fast local level set method," *Comput. Phys.,* vol. 155, pp. 410-438, 1999.

[26] F. Ilnicki, P. Sobieszuk and R. Pohorecki, "SIMULATIONS OF A TWO PHASE FLOW IN A CLOSED MICROCHANNEL," *Chem. Proc. Eng.,* vol. 30, pp. 205-216, 2009.

[27] L. Zheng and H. Zhang, "An adaptive level set method for moving-boundary problems: application to droplet spreading and solidification," *Numerical Heat Transfer Part B: Fundamentals,* vol. 37, pp. 437-454, 2000.

[28] J. Lienemann, A. Greiner and J. G. Korvink, "Modeling, simulation, and optimization of electrowetting," *IEEE Transactions on Computer Aided Design of Integrated Circuits and Systems,* vol. 25, pp. 234, 2006.

[29] M. Abdelgawad and A. R. Wheeler, "Low-cost, rapid-prototyping of digital microfluidics devices," *Microfluidics and Nanofluidics,* vol. 4, pp. 349-355, 2008.

[30] M. Abdelgawad and A. R. Wheeler, "Rapid prototyping in copper substrates for digital microfluidics," *Adv Mater,* vol. 19, pp. 133–137, 2007.

[31] M. Abdelgawad and A. R. Wheeler, "3D droplet actuation in digital microfluidics devices," in *Solid-State Sensors, Actuators and Microsystems Conference, 2007. TRANSDUCERS 2007. International,* 2007, pp. 1809-1812.

[32] A. Bateni, S. S. Susnar, A. Amirfazli and A. W. Neumann, "A high-accuracy polynomial fitting approach to determine contact angles," *Colloids Surf. Physicochem. Eng. Aspects,* vol. 219, pp. 215-231, 2003.

[33] C. G. Cooney, C. Y. Chen, M. R. Emerling, A. Nadim and J. D. Sterling, "Electrowetting droplet microfluidics on a single planar surface," *Microfluidics and Nanofluidics,* vol. 2, pp. 435-446, 2006.

[34] C. Roero, "Contact angle measurements of sessile drops deformed by a DC electric field," in *Proc. of 4th International Symposium on Contact Angle, Wettability and Adhesion, Philadelphia, USA,* 2004.